THE NITROGEN ION LASER

Carl B. Collins, et al

Texas University

Prepared for:

Office of Naval Research
Advanced Research Projects Agency

1 October 1974

Security Classification

DOCUMENT CONTROL DATA - R & D AD/A 002484

(Security classification of title, body of abstract and indexing annotation must be entered when the overall report is classified)

1. ORIGINATING ACTIVITY (Corporate author)
The University of Texas at Dallas
P. O. Box 688
Richardson, Texas 75080

2a. REPORT SECURITY CLASSIFICATION
UNCLASSIFIED

2b. GROUP

3. REPORT TITLE
THE NITROGEN ION LASER

4. DESCRIPTIVE NOTES (Type of report and inclusive dates)
Fifth Semi-Annual Technical Report (Period covered: 3/1/74-9/30/74)

5. AUTHOR(S) (First name, middle initial, last name)
Carl B. Collins
Austin J. Cunningham

6. REPORT DATE
1, October 1974

7a. TOTAL NO. OF PAGES
91

7b. NO. OF REFS
23

8a. CONTRACT OR GRANT NO
N00014-67-A-0310-0007

b. PROJECT NO
ARPA Order No. 1807

c.
Program Code 2E90

d.

9a. ORIGINATOR'S REPORT NUMBER(S)
UTDP ML-02

9b. OTHER REPORT NO(S) (Any other numbers that may be assigned this report)
A 002-5

10. DISTRIBUTION STATEMENT
Distribution of this document is unlimited

11. SUPPLEMENTARY NOTES

12. SPONSORING MILITARY ACTIVITY
Office of Naval Research

13. ABSTRACT

The characterization of the nitrogen ion laser pumped by charge transfer from He_2^+ is reported in this work. Intense laser emission in the violet at 427 nm has been observed and found to have a linewidth less than 0.3 A. The pumping ion, He_2^+, was produced by discharge of a fast-pulsed electron beam gun, APEX-1, into 7 atmospheres of a mixture of helium and nitrogen. Excitation current densities were 1.4KA/cm^2 at 1 MV over a 1 x 10 cm transverse geometry. Under these conditions, the efficiency of the emission of 427 nm laser radiation was found to be 1.8% relative to the energy lost by the electron beam in the radiating volume for small volumes and 0.3% for volumes of the order of 25cc. Efficiency is found to be the same as that of an argon nitrogen excitation transfer laser operating at the same level of energy deposition.

DD FORM 1 NOV 68 1473

Security Classification

14. KEY WORDS	LINK A		LINK B		LINK C	
	ROLE	WT	ROLE	WT	ROLE	WT
Nitrogen Ion Laser						
Charge Transfer						
Laser						

Fifth Semi-Annual Technical Report

Item A002

Period Ending 30, Sept. 1974

Short Title: RECOMBINATION LASER

ARPA Order Number 1807

Program Code Number 2E90

Contract Number N00014-67-A-0310-0007

Principal Investigator: Carl B. Collins
The University of Texas at Dallas
P. O. Box 688
Richardson, Texas 75080
(214) 690-2885

Contractor: The Board of Regents of
The University of Texas System

Scientific Officer: Director
Physics Programs
Physical Sciences Division
Office of Naval Research
Department of the Navy
800 N. Quincy Street
Arlington, Virginia 22217

Effective Date of Contract: 21 March 1972

Expiration Date of Contract: 30 June 1975

Amount of Contract:	$ 99,990.00
Amount of Modification #1:	91,400.00
Amount of Modification #2:	100,000.00
Amount of Modification #3:	150,000.00
Total Amount:	$441,390.00

Sponsored by

Advanced Research Projects Agency

ARPA Order No. 1807

Form Approved Budget Bureau No. 22-R0293

CONTENTS

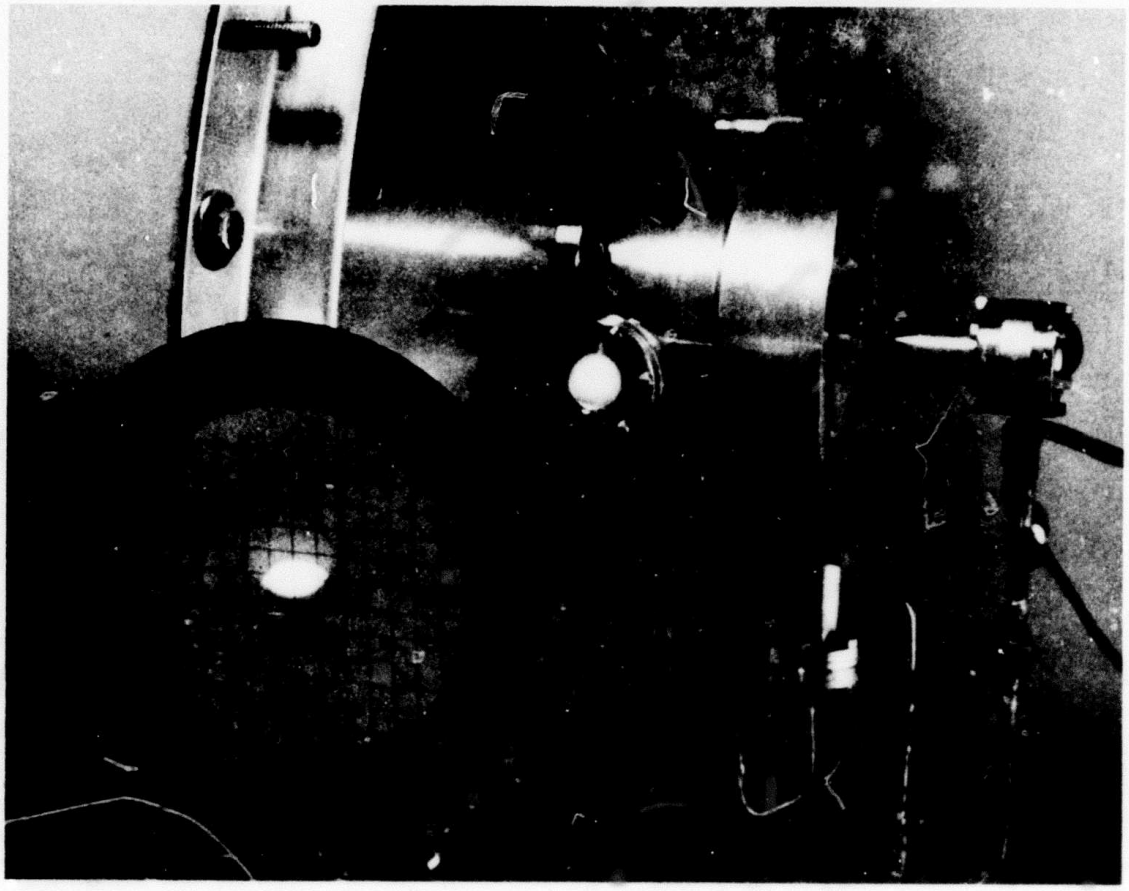

Emission from the first nitrogen ion laser. The output beam is seen in the photograph striking the ruled translucent target in the lower left. The emission consists of a single spectral line of less than 0.3 Å linewidth at 4278 Å in the violet. The laser cavity is contained in the pressure vessel with sapphire windows sealed across the optical axis. It is the most efficient visible laser constructed to date scaling at 0.3% of the electron beam energy deposited in the gas.

I. TECHNICAL REPORT SUMMARY

It was recently proposed by Collins, et.al.[1] that resonant charge transfer reactions might provide nearly ideal pumping mechanisms for recovering one photon for each ion produced by the discharge of an intense electron beam into high pressure gases. Since the energy from an e-beam discharge can be stored at densities of the order of kilojoules per liter with efficiencies over 50%, such a pumping mechanism would clearly point toward the development of e-beam lasers operating at visible wavelengths with system efficiencies between 5 and 10%. The potential of the pumping reaction

$$He_2^+ + N_2 \rightarrow N_2^+ (B^2\Sigma_u^+) + 2He, \qquad (1)$$

was reported in the same letter[1], together with construction of a two-pass amplifier excited by a Febetron 706 and operating at 4278, 4709 and 5228 Å. The first nitrogen ion laser pumped by charge transfer from He_2^+ was subsequently constructed as described in a recent letter[2]. Intense laser emission at 4278 Å was reported with an efficiency measured to be 1.8% relative to the energy lost by the electron beam in a relatively small radiating volume of 0.63 cm^3. A peak output power of 9.1 KW was achieved.

Subsequent studies of the dependence on experimental parameters of the power output have demonstrated that the nitrogen ion laser scales with pressure and volume at a rate more consistent with an efficiency of 0.3% relative to the energy lost by the electron beam. This is the same as the efficiency found for the argon-nitrogen, excitation transfer laser when optimized for the same conditions. Such comparison of relative efficiency of nitrogen laser types under

similar conditions provides a particularly useful normalization of measurement since the determination of absolute energy deposition is generally unconvincing at the present state-of-the-art.

The laser device used in these studies consisted of a pair of plane dielectric mirrors which were mounted to allow angular alignment, spaced with 14 cm invar rods, and contained in a stainless steel pressure vessel with sapphire windows sealed across the optical axis external to the cavity. In operation the system was filled to a pressure ranging from 1 to 14 atmospheres of a mixture of either helium and nitrogen or argon and nitrogen. Useful partial pressures of nitrogen ranged from 2 to 30 Torr in the case of helium and from 350 to 700 Torr in the case of argon. Excitation was provided by an electron beam entering through a supported, 0.002-in thick titanium foil window and propagating in a direction perpendicular to the optical axis. The cross section of the beam was 1 cm x 10 cm with the longer transverse axis coincident with the optical axis of the cavity. The electron beam was emitted by APEX-1, pulsed at 14 KA and 950 KV for a duration of 20 nsec with rise and fall times of 7 nsec.

Spectra were recorded with a Spex 0.75 m spectrograph with 5μ slits. Resolution was limited in practice to about 0.3 Å by the resolution of the Polaroid film used. The time dependence and power level of the light output was measured with a calibrated ITT F-4000, S20 vacuum photodiode connected directly to a Tektronix 519 oscilloscope. Proper attenuation of the laser output was provided by calibrated neutral density filters.

In operation intense laser emission from the helium nitrogen mixtures was observed in the violet at 4278 Å and found to have a linewidth less than 0.3 Å. Beam divergence was measured to be 3 milliradians from photographs of the illuminated spot on targets successively placed at distances varying from 1 to 10 m.

Examination of the spectrum of the laser emission showed primarily the single line at 4278 Å corresponding to the band head in the P-branch of the (0,1) vibrational transition of the $B^2\Sigma_u^+ \rightarrow X^2\Sigma_g^+$ electronic transition of the nitrogen molecular ion, N_2^+. With the proper mirror set this could be suppressed and the (0,0) transition at 3914 Å could be forced to lase. In this case self-termination occurred much more rapidly than for the (0,1) transition suggesting the importance of some collisional mechanism preferentially depopulating the lower $v''=1$ laser level.

The radiating volume in the earliest tests with a concave mirror set was estimated to be 0.63 cm^3 from application of a double cone geometry to enlarged photographs of the illuminated spot at the base of the cone on the output dielectric mirror, and from this energy densities corresponding to the observed output were calculated. A more direct calibration of the radiating volume was possible in the scaling studies conducted with the plane mirror geometry. In these cases the radiating volume was 25 cm^3 and the peak power extracted at 4278 Å was 325 KW at 13.4 atmospheres of pressure.

A summary of output pulse energies as functions of energy deposition is seen in Figure 1. Deposition is shown in normalized units in which for helium, dE/dx is assumed to be 1.0. The relevant deposition time can be estimated from the time required for the laser output to fall to 1/e of its peak value, and for helium this also has been normalized to unity. As a consequence, the relative deposition is equal to the total gas pressure for helium. On such a plot, then, lines of constant efficiency appear as diagonals.

As can be seen, not only output pulse energy, but also efficiency emerges strongly with energy deposition from the e-beam, most probably as a consequence of unblocking of the lower state by collisional processes involving free electrons.

Figure 1

Summary plot of total laser pulse energy emitted from a 25 cm^3 volume as a function of relative deposition of energy from the electron beam. Variation of the deposition is obtained by changing the total gas pressure; hence the stopping power. The peak e-beam current is 14 KA in each case. Lines of constant efficiency appear as diagonals.

○ - Helium containing 8 Torr nitrogen

□ - Helium containing 20 Torr nitrogen

Δ - Argon containing 646 Torr nitrogen

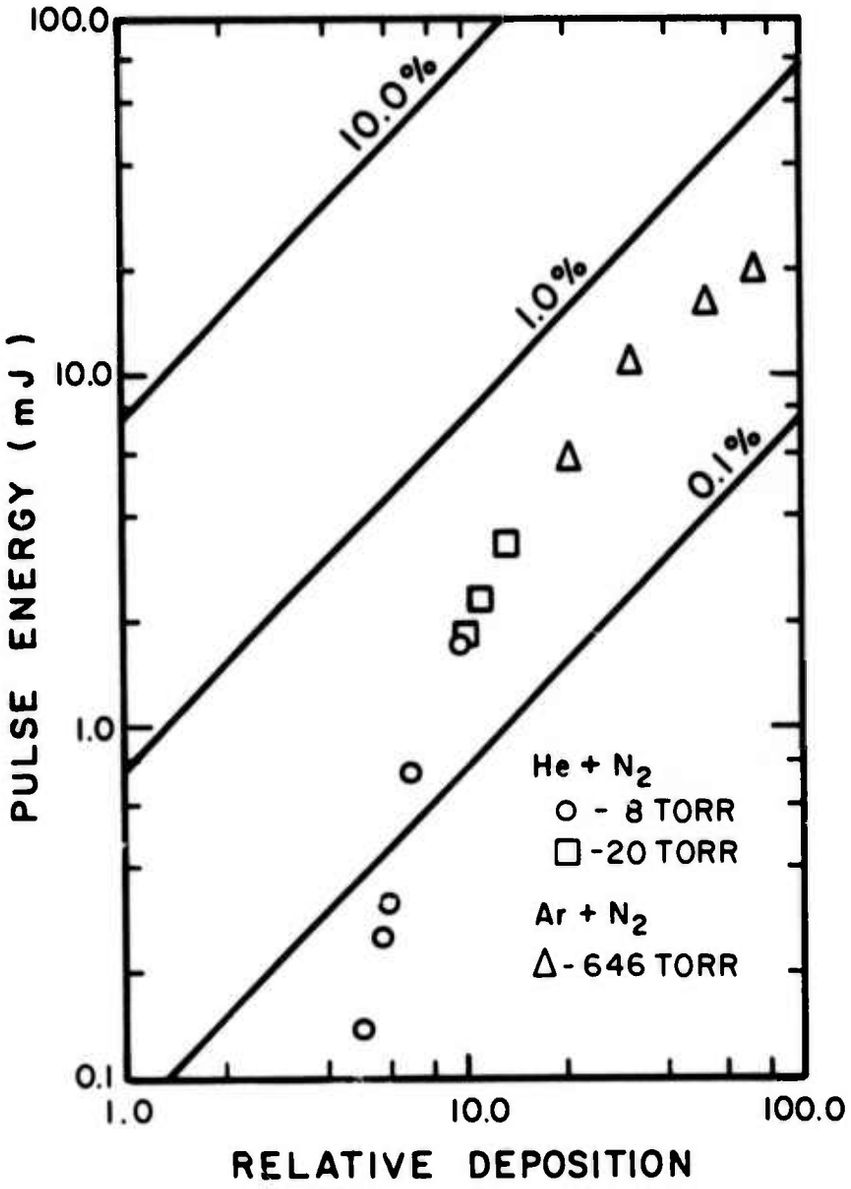
100.0
10.0
1.0
0.1
PULSE ENERGY (mJ)
10.0%
1.0%
0.1%
He + N2
O - 8 TORR
□ -20 TORR
Ar + N2
Δ - 646 TORR
1.0
10.0
100.0
RELATIVE DEPOSITION

Efficiencies of 0.3% are reached at 13.4 atmospheres and 14 KA. Whether the upward trend continues can only be resolved by measurements at higher depositions. In any case it can be seen that the efficiency reached at 13.4 atmospheres is the same efficiency characteristic of the argon-nitrogen, UV laser operated at substantially higher levels of energy deposition.

Although promise of the nitrogen ion laser is clearly of such importance that substantial continuing effort to optimize its performance is warranted, it must be realized that it is only the first example of the new class of e-beam lasers pumped by charge transfer[1] and other similar systems offer the possibilities of even higher efficiencies and broader selections of output wavelengths. Nevertheless, the high efficiency already observed for the emission of 4278 Å laser radiation from this system points to the nitrogen ion laser as a device of considerable significance and clearly confirms the importance of charge transfer reactions as laser pumping mechanisms.

II. THEORY

The development of intense pulsed electron beam sources in the 1 to 100 Gigawatt class have made feasible the deposition of energy in the form of ionization into large volumes of plasma with system efficiencies around 50%. Given an elementary mechanism utilizing this ionization and leading to the inversion of population at quantum efficiencies which are typically 10 to 20%, overall radiative efficiencies of the order of 5 to 10% can be realistically projected, provided the plasma constituents are arranged to allow for the domination of the desired reaction channel. The xenon excimer laser [3,4] is the best example of such a system in which the primary mechanism is the dissociative recombination of the Xe_2^+ ion. Though superficially similar, the electron beam excited pure N_2 [5] and H_2 [6] lasers do not actually utilize the primary ionization of the plasma; consequently, system efficiencies are reduced by orders of magnitude.

Evidently, charge transfer between the population of primary ions and a minority constituent of lower ionization potential offers a nearly ideal mechanism [1] for ultimately obtaining one photon per primary ion. If the minority constituent is selected to have the energy of an excited state of its ion approximately equal to that of the primary ion, in principle, one photon per ion can be realized with a quantum efficiency, E, equal to

$$E = \frac{IP(1)-IP(2)}{IP(1)} \qquad (2)$$

where IP(1) and IP(2) are the ionization potentials of the primary and secondary constituent, respectively. Table 1 summarizes examples of possible system efficiencies characteristic of various permanent gases diluted in helium.

TABLE 1

Projected system efficiencies for the emission of radiation following charge transfer excitation from the helium molecular ion, assuming a 50% efficiency for the production of ionization by electron beam impact.

Minor Constituent	Overall Efficiency
N_2	11.0%
O_2	12.5%*
CO	14.5%

*The resonant transition does not terminate on the ground state of the molecular ion.

Similar possibilities occur with other primary species, but at efficiencies reduced by the lower ionization potential of those species.

Both the available output energy and pulse duration depend strongly on partial pressures, and the high values of charge density which become feasible with e-beam excitation are needed. The deposition of energy into a high pressure gas by an electron beam is a very complex problem, and most characterizations of the process have been made for the excitation of dense inert gases. In such systems as xenon, beam-plasma effects rapidly dominate with the return currents[7,8] playing a large role. However, in the singular case of the light inert gases at beam currents below 20 KA, simplifying assumptions exist which render the problem tractable. Subject to limitations on the product of gas density and beam penetration depth, to be discussed below, the problem can be resolved into that of the differential energy loss in the gas of β-particles in a beam, the morphology of which is completely determined by the foil window through which the beam has entered.

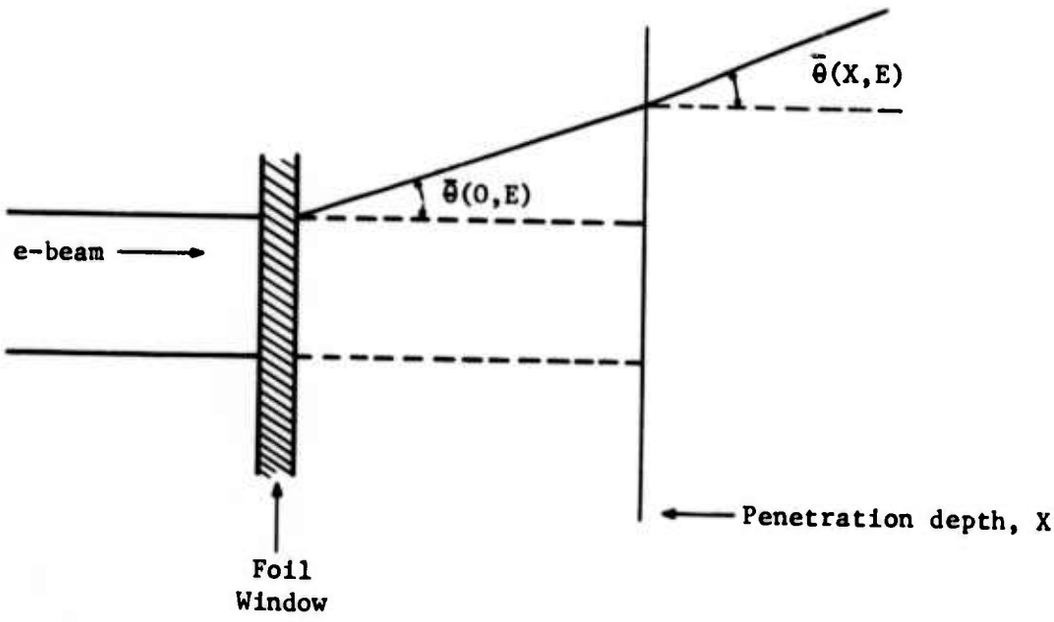

Figure 2: Schematic drawing of electron beam injection into high pressure gas sample.

Referring to Fig. 2, the mean scattering angle $\bar{\theta}(E)$ of electrons exiting from the foil window can be readily calculated for the case of "multiple scattering,"[9] which corresponds to that descriptive of foils of realistic dimensions. After some distance of penetration, X, into the gas, the mean scattering angle has increased to a value $\bar{\theta}(X,E)$. To determine the conditions under which $\theta(X,E)$ differs significantly from $\bar{\theta}(0,E)$, assume

$$\bar{\theta}(X_E,E) \geq 1.1\ \bar{\theta}(0,E) \quad , \tag{3}$$

which means that at the critical depth of penetration, X_E, for that energy, E, the root-mean-square scattering angle is increased 10%. Since angles of magnitude $\bar{\theta}(0,E)$ are characteristic of multiple scattering conditions, it is reasonable and consistent to assume those of $\bar{\theta}(X_E,E)$ are similarly characteristic. Expressions for $\bar{\theta}(X,E)$ are tedious though well-established[9] and substitution into (3) yields for a titanium foil, .002" thick, after simplification the following bounds on the domain of gas transparency,

$$PX \text{ (Helium)} \leq 273 \text{ atm. cm} \qquad (4a)$$

$$PX \text{ (Argon)} \leq 4.3 \text{ atm. cm} \quad . \qquad (4b)$$

It can be seen from these results that, whereas the simplifying assumptions break down for argon (Z=18) at an inch of penetration at two atmospheres, they remain valid in helium (Z=2) over the entire span of parameters required for practical operation of a small test laser device. For example, at 30 atmospheres pressure, the simplified model is valid to at least 9.1 cm depth of penetration which is sufficient to describe about a half liter volume excited by a 1 x 10 cm electron beam of divergence characteristic of transmission through a .002" titanium foil window at 1 MeV for currents less than 20 KA. At higher currents, the "drag e.m.f."[8] resulting from the return currents should be considered.

In the following material the theoretical model derived will be understood to be subject to the restrictions

$$E \leq 1 \text{ MeV} \qquad (5a)$$

$$I_o \leq 20 \text{ KA} \qquad (5b)$$

$$PX \leq 280 \text{ atm. cm} \qquad (5c)$$

and the beam input to the foil window will be assumed to have a 1 x 10 cm transverse cross-section.

Since it will now be assumed that the beam propagation in the high pressure gas has been determined by the scattering in the foil window, an examination of the resulting beam divergence is necessary. For the conditions of multiple scattering which apply in the most practical conditions considered here, the distribution of scattering angles is unambiguous[9] and what is needed, then, is the most probable path length of an electron emerging from the foil per centimeter of penetration depth X, measured normal to the window foil.

Figure 3 presents the solutions[10] for the mean path length in terms of the angle $\bar{\psi}$ at which the electron traverses a path of "average length" in penetrating to a depth X. Notice that $\bar{\psi} \neq \bar{\theta}$ for either of the two depths of penetration shown. However, for large $\bar{\theta}$, the scattering is more probably described by diffusion[9] of the electron beam through the foil and this limiting case is shown in Figure 3 as the dashed limit and, in fact, must represent an asymptote to $\bar{\psi}$ as a function of $\bar{\theta}$. As $\bar{\theta}$ increases, the type of scattering must pass smoothly from "multiple" to saturated diffusion, and since the intermediate case of scattering is quite difficult to treat exactly, the graphical interpolation shown by the heavy solid curve of Figure 3 was constructed for use in the theoretical model. In practice the transition region between 40° and 60° corresponds to the energy range of 0.5 to 0.3 MeV for a .002" thick titanium foil and so is of significance for a relatively small interval of time on the leading and the trailing edge of the e-beam pulse. This, coupled with the small difference in the $\bar{\psi}$'s obtained from the two models of large angle scattering, limits errors resulting from the use of the graphical interpolation to a few percent.

To determine the scattering angle as a function of beam energy, the functional dependence of $\bar{\psi}$ on E was determined[10] as shown in Figure 4.

Figure 3

Graph of mean path angle, $\bar{\psi}$, as a function of the mean scattering angle, $\bar{\theta}$.

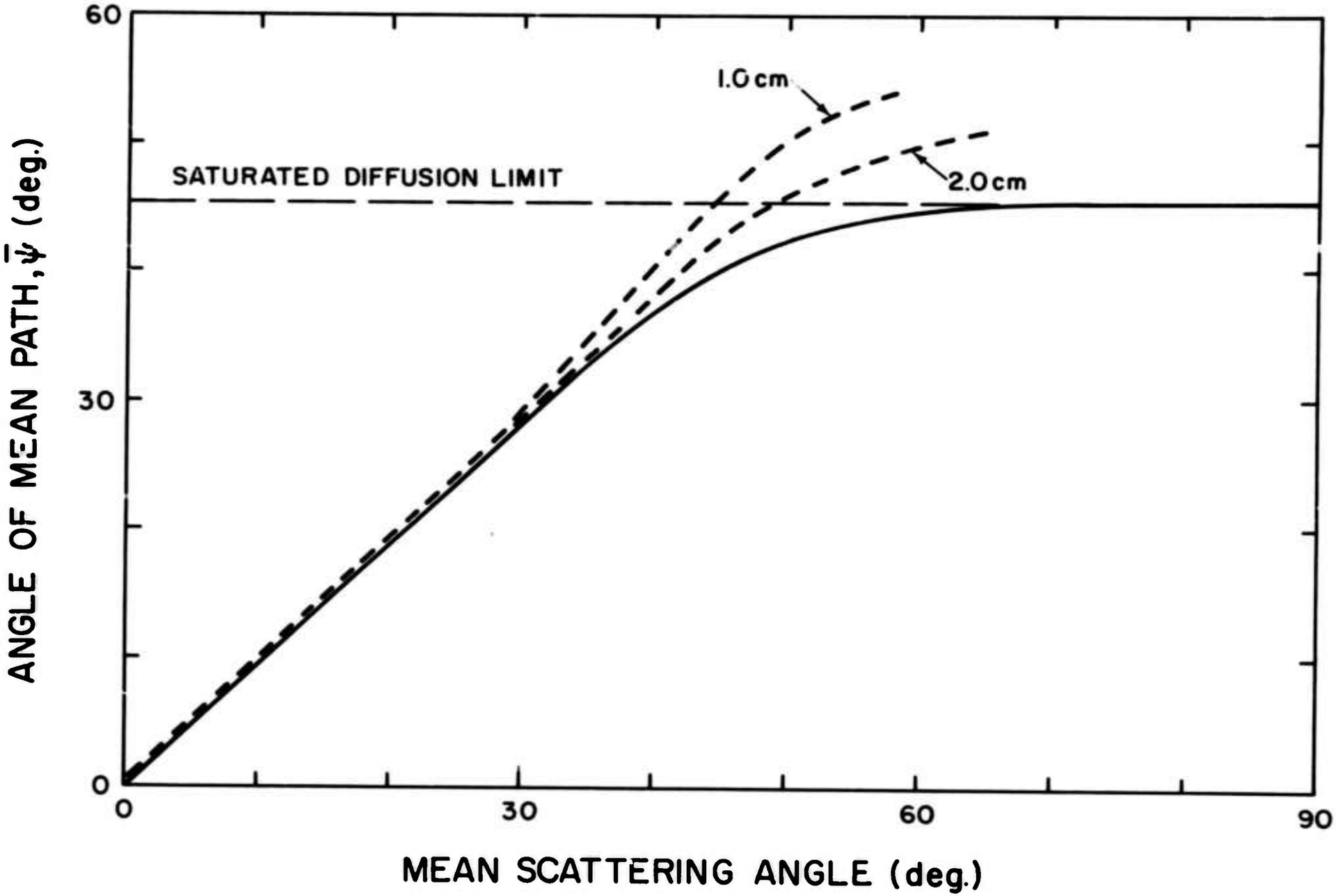
60
30
0
0
30
60
90
1.0 cm
2.0 cm
SATURATED DIFFUSION LIMIT
ANGLE OF MEAN PATH, $\bar{\psi}$ (deg.)
MEAN SCATTERING ANGLE (deg.)

Figure 4

Graphs of mean path angle, $\bar{\psi}$, and beam attenuation as functions of e-beam energy input to the .002" thick Ti foil. The ordinate scale is common to both graphs and units for each are shown in parentheses.

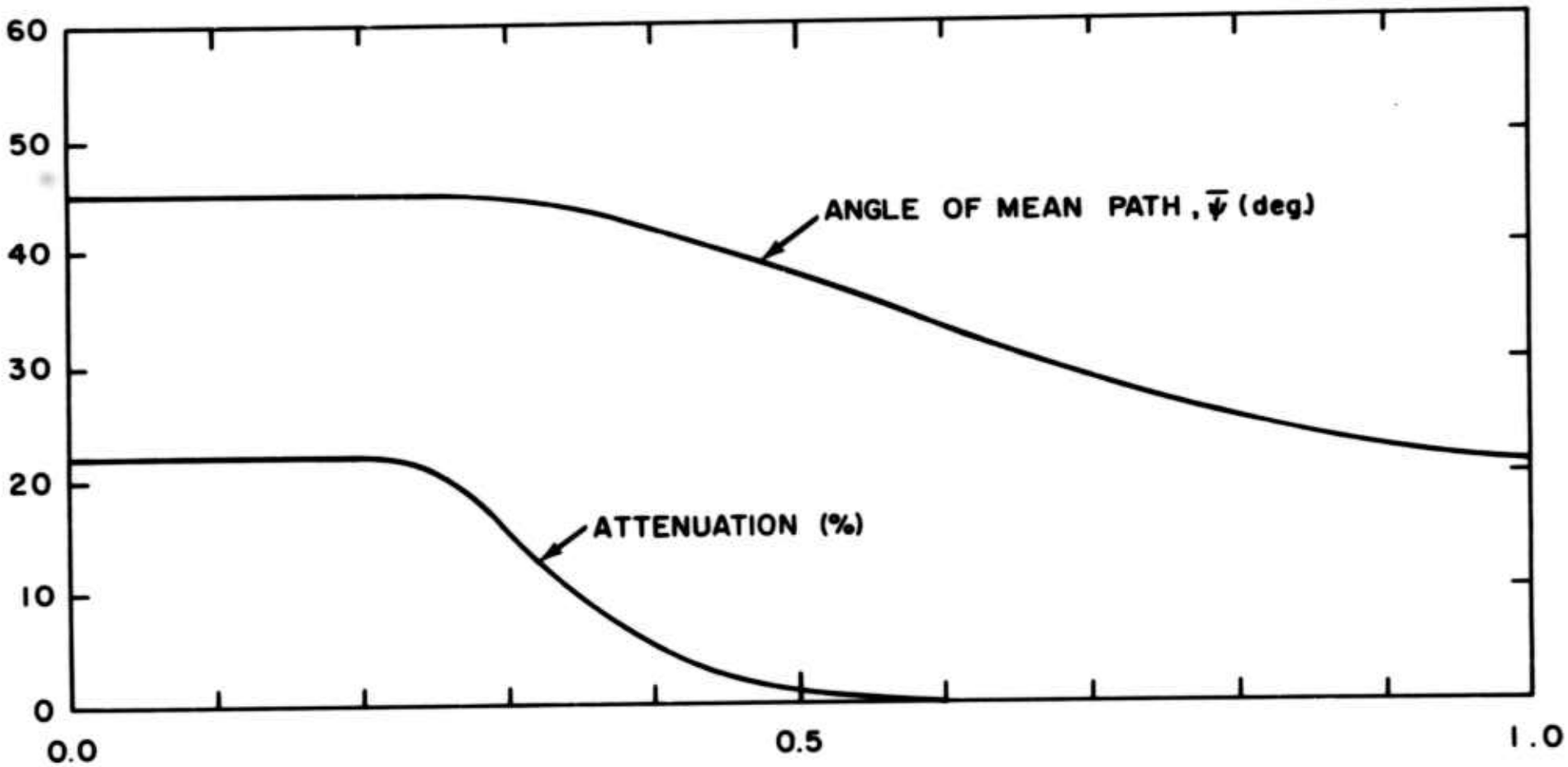
60
50
40
30
20
10
0
0.0
0.5
1.0
ANGLE OF MEAN PATH, $\bar{\psi}$ (deg)
ATTENUATION (%)
INPUT E-BEAM ENERGY (MeV)

At relativistic energies, the beam energy lost in the foil can be expressed simply as the Bethe-Block expression for the differential energy loss multiplied by the mean path length in the foil. At lower energies ΔE can become a significant fraction of the beam energy and the non-relativistic expression for the differential energy loss must be used. Finally the energy of the beam emerging from the foil can be written in terms of the beam energy input, E. Then the energy deposition in the gas can be approximated by the expression

$$\Delta E = \left(-\frac{dE}{dx}\right) \Delta X \left(\cos \bar{\psi}\right)^{-1} \quad , \tag{6}$$

where dE/dx is a rather complex function of initial e-beam energy[10] and $\bar{\psi}$ is the function shown in Figure 4.

Combining, then, the data calculated gives differential energy loss per unit penetration depth as a function of electron beam energy input to the .002 inch thick foil window of an experimental device. Values of this function are plotted in Figure 5 in units of KV/atm/cm for various input e-beam energies. Over a small range of E_o, ΔE computed according to (6) exceeded the energy E(x) of the emerging beam. For those values of E_o, E was replaced by E(x) in accordance with the assumption that all the energy of the emerging beam is stopped in the experimental volume bounded by the penetration depth ΔX.

The spike seen in Figure 5 corresponds to those conditions for which most of the beam energy is deposited in the foil and the beam emerges at low velocity giving a relatively large (-dE/dx). However, since in the cases considered here the beam spends relatively little time at those energies, the total ionization resulting from those conditions is small.

The power deposition per unit volume can be written by considering that the energy lost by the beam in penetrating to a depth X is deposited in a rectangular pyramid with its sides slanting with angle $\bar{\psi}$ away from the beam axis,

Figure 5

Graph showing the differential energy loss per unit penetration depth in helium in units KV/cm/atm as a function of electron beam energy input to a 0.002 inch thick Ti foil window of the experimental device.

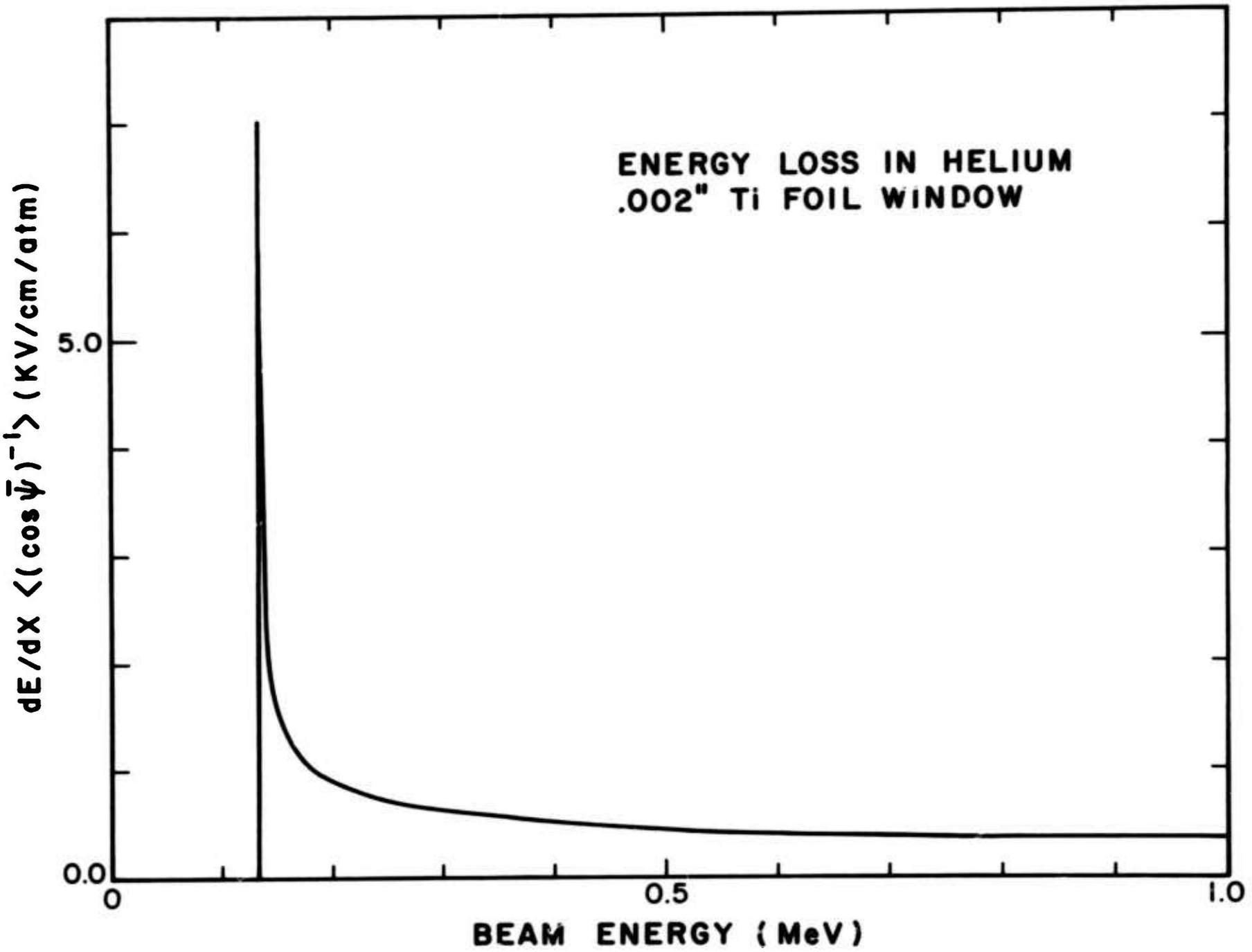
ENERGY LOSS IN HELIUM
.002" Ti FOIL WINDOW
dE/dX <(cosψ̄)⁻¹> (KV/cm/atm)
5.0
0.0
0
0.5
1.0
BEAM ENERGY (MeV)

truncated at the foil surface and having its base on the plane located a distance X from the foil and normal to the beam axis. The volume of such a figure is

$$\Delta V = X\,[10 + X\,(11 \tan \bar{\psi} + 4/3 \tan^2 \bar{\psi})] \quad , \qquad (7)$$

and depends on beam energy, E_o, through $\bar{\psi}$. Then the energy deposition can be written

$$d\varepsilon\,(X,E_o) = \frac{I_o\,(t)\,[1\text{-Att}\,(E_o)]}{10 + [11 \tan \bar{\psi}\,(E_o) + 4/3 \tan^2 \bar{\psi}\,(E_o)]X} \cdot$$

$$\left\{ - \frac{dE}{dx}\,(E_o)\,(\cos\bar{\psi}(E_o))^{-1} \right\} dt \quad , \qquad (8)$$

where the term in braces is that shown in Fig. 5 and 1-Att can be obtained from Fig. 4. The beam current $I_o(t)$ can be written in terms of $E_o(t)$ and a constant Ω, by assuming

$$I_o(t) = \frac{1}{\Omega} E_o\,(t) \quad . \qquad (9)$$

Further assuming the beam energy has a time dependence,

$$E_o(t) = \begin{cases} (t/\tau)\ \text{MeV} & \text{for } t \leq \tau \\ 1\ \text{MeV} & \text{for } t > \tau \end{cases} \quad , \qquad (10)$$

and $dt = \tau dE$ where E is in MeV and $t \leq \tau$. Then the energy deposited in the experimental volume, ΔV by the time t is

$$\varepsilon\,(t) = \int_o^t d\varepsilon \qquad (11)$$

which can be written in terms of an ionizing function

$$F(E) = E \frac{[1-Att]}{\left(\frac{\Delta V(E,X)}{X}\right)} \left[-\frac{dE}{dx}(E). (\cos \bar{\psi}(E))^{-1} \right] , \qquad (12)$$

as

$$\varepsilon(t) = \frac{\tau_N}{\Omega} \int_0^E F(E')dE' \ (\text{Joules}/\ell/\text{atm}), \qquad (13)$$

where τ_N is the risetime in nanoseconds and Ω is now 1 MeV/I_o where I_o is the maximum beam current in amps. F(E) is plotted for helium for the case X=2cm in Fig. 6 and serves as a model for obtaining the energy expended by the time the beam energy has risen to a value E_o following initiation of the e-beam discharge. For times $t > \tau$ the beam energy is constant, as is the power deposition, and $d\varepsilon$ becomes

$$d\varepsilon = \frac{126}{\Omega}(\text{Joules}/\ell/\text{nsec}) . \qquad (14)$$

The cumulative energy deposition can then be calculated, once the time dependence of the input e-beam is known, by integrating the deposition function of Fig. 6 for $t < \tau$. For times greater than τ, the value of

$$\int_0^{\tau} d\varepsilon = 8.65\ \tau_N/\Omega \ (\text{J}/\ell/\text{atm}) , \qquad (15)$$

can be used to describe the total deposition on the leading edge of the pulse. Then to $t = T_N$, the time bounding the end of the plateau (in nanoseconds),

Figure 6

Logarithmic graph of ionizing function, F(E) defined in eq. (32) for helium as a function of e-beam energy input to the .002" thick Ti foil. The integral of this curve multiplied by τ_N/Ω give the energy deposition in Joules/liter/atm.

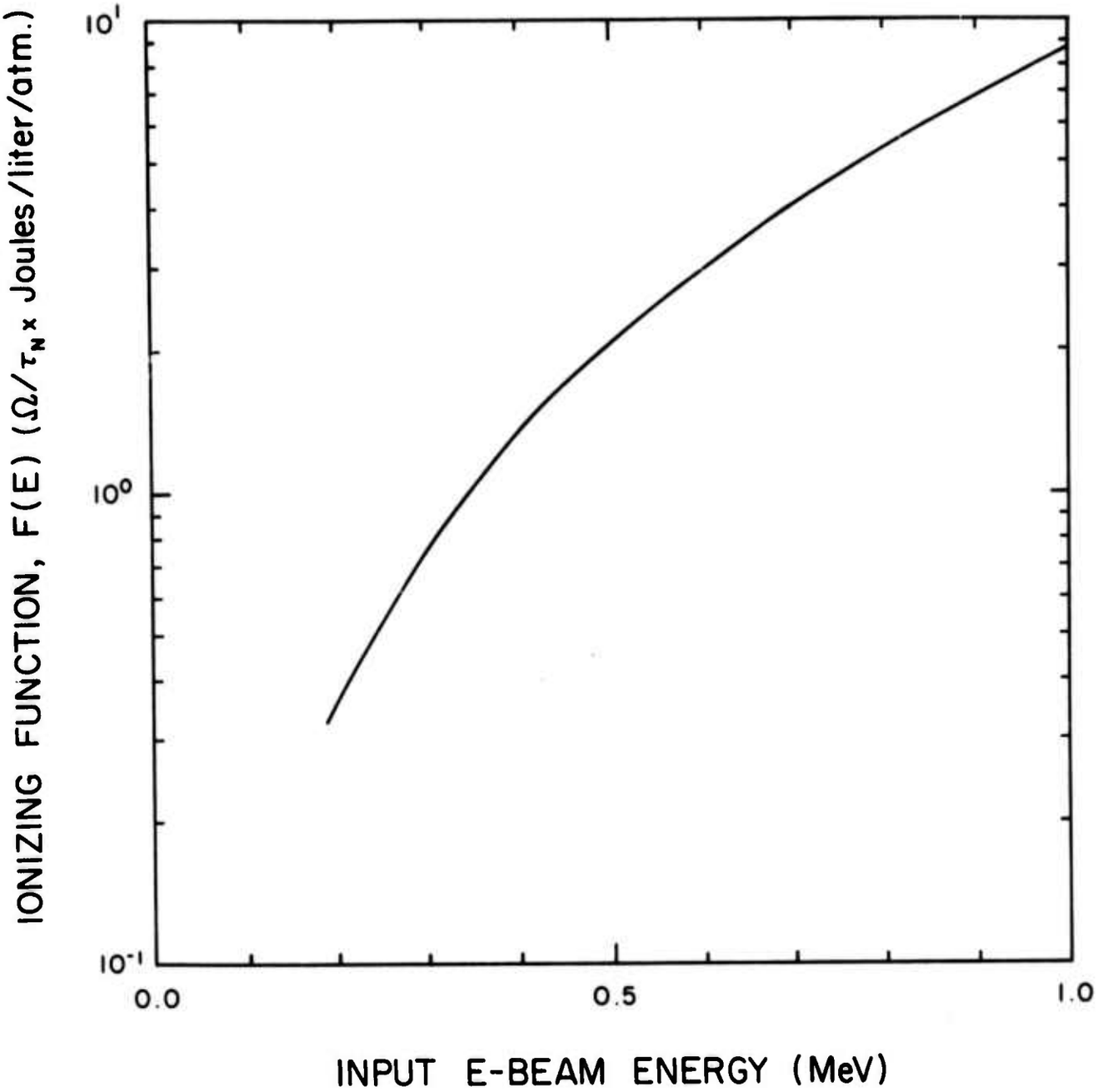
IONIZING FUNCTION, F(E) (Ω/τ_N x Joules/liter/atm.)
10^1
10^0
10^{-1}
0.0
0.5
1.0
INPUT E-BEAM ENERGY (MeV)

$$\varepsilon(t) = 8.65\ \tau_N/\Omega + 18.05\ (T_N - \tau_N)/\Omega \text{ (Joules/}\ell\text{/atm)}, \quad (16)$$

provides a reasonable model. Finally considering, for simplicity, the tail of the pulse to be a linear decay similar to the leading edge,

$$\varepsilon = 17.3\ \tau_N/\Omega + 18.05\ (T_N - \tau_N)/\Omega \text{ (Joules/}\ell\text{/atm)}. \quad (17)$$

For APEX-1, the electron beam device used in these experiments,

$$\tau_N = 6.6 \text{ nsec}, \quad (18a)$$

$$T_N = 20 \text{ nsec}, \quad (18b)$$

and Ω^{-1} can be written for a 1 MeV maximum output

$$\Omega^{-1}/I = 10^{-3}\ (KA)^{-1} \quad . \quad (19)$$

Then

$$\varepsilon = 0.356 \text{ Joules/}\ell\text{/atm/KA} \quad . \quad (20)$$

This can be related to the ionization produced by recognizing that the energy cost per ion in helium[11] is 42.3 eV and that 1 Joule/ℓ will produce 1.478×10^{14} ions/cm^3. The energy stored as ionization is 24.5 eV per ion so that the efficiency of energy storage is

$$\text{Eff} = 57.9\% \quad . \quad (21)$$

Table 2 summarizes the energy storage which can be achieved in helium excited by APEX-1, a 100 KA, 1 MeV, e-beam device pulsed typically for 20 nsec FWHM with 6.6 nanosecond rise and fall times.

TABLE 2

Summary of the energy density stored as ionization in high pressure helium following discharge of APEX-1. The efficiency of the storage relative to the total energy deposited by the beam is 57.9%.

	ENERGY DENSITY (JOULES/LITER)	
Beam Current	20 KA	100 KA
Pressure		
3 atm	12.4	62
30 atm	124	620

The ionization produced can be obtained from Table 3 by noting that 1 Joule/ℓ stored as He^+ represents 2.55×10^{14} ions/cm^{-3}. According to (21), an elementary mechanism utilizing this ionization and leading to the inversion of population would make possible overall radiative efficiencies about half of the absolute quantum efficiency of the transition. In the visible wavelength region, this would mean efficiencies between 5 and 10%, provided the plasma constituents could be arranged to allow for the domination of the desired reaction channel.

Evidently, a resonant charge transfer reaction between the population of primary ions in the plasma and a minority constituent of lower ionization potential offers a nearly ideal mechanism for ultimately obtaining one photon per primary ion. Fig. 7 presents the energy level diagrams of the ions of helium and nitrogen. Studies[12] on low pressure charge transfer mixtures have shown the strong development of spectra from molecular ion levels in near resonance with the primary helium ions. One such selectively excited transition is indicated by the arrow in Fig. 7 . Particular charge transfer reactions are of the form

$$He^+ + XY \rightarrow (XY^+)^* + He \qquad (22a)$$

$$\rightarrow X^+ + Y + He \qquad (22b)$$

and

$$He_2^+ + XY \rightarrow (XY^+)^* + 2He \qquad (23)$$

where the asterisk indicates additional electronic excitation. Although quantum efficiencies are more favorable for reactions excited by He^+, in practice the importance of channel (22b) in the case of N_2 minimizes the importance of the He^+ ion.

At sufficiently high pressure, the He^+ is rapidly converted to He_2^+ by the termolecular reaction

Figure 7

Energy level diagrams for the ionic states of helium and molecular nitrogen.

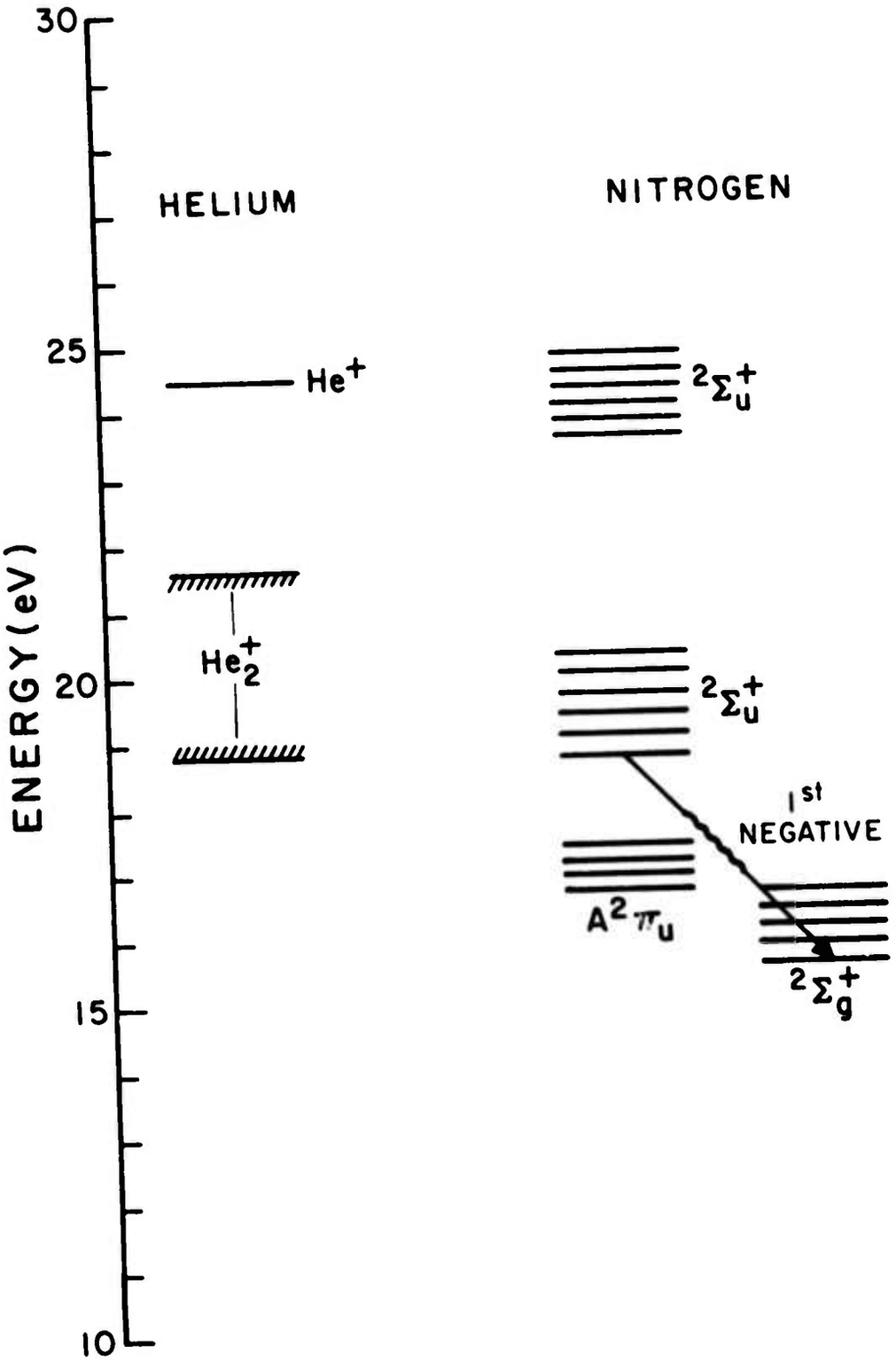
30
25
20
15
10
ENERGY (eV)
HELIUM
NITROGEN
He+
He2+
2Σu+
2Σu+
1st
NEGATIVE
A2πu
2Σg+

$$He^+ + 2He \rightarrow He_2^+ + He \qquad (24)$$

with a characteristic lifetime of

$$\tau = \frac{27}{p^2} \text{ nsec}^{13} \qquad (25)$$

where p is in atmospheres. Provided the partial pressure of minority constituent is not too great for reaction (24) to go to completion, the ionization will convert from He^+ to He_2^+, thus making available the charge transfer reaction

$$He_2^+ + N_2 \rightarrow (N_2^+)^* + 2He \qquad . \qquad (26)$$

This reaction[14] has a rate coefficient of about 10^{-9} cm^3 sec^{-1} as does the analogous reaction[15] with He^+.

Requiring, then, a low enough partial pressure of minority gas so that reaction (24) can reach an $(1-e^{-1})$ end-point yield in competition with the competing channel for the loss of He^+ through unwanted charge transfer sets the upper limits on the partial pressures shown in Table 3.

TABLE 3

Partial pressures of He and diatomic admixtures to allow for a conversion of a fraction of $(1-e^{-1})$ of He^+ to He_2^+ in competition with charge transfer of He^+ and the resulting charge transfer lifetimes.

He	Max Admixture	Charge Transfer Lifetimes
3 atm	5.9 Torr	5.3 nsec
30 atm	590 Torr	0.05 nsec

Assuming that the lifetime of the source term for the minority excited states limits the rate at which energy can be extracted from the plasma through a stimulated transition, the minimum pulse widths can be computed from the partial pressures and these are shown in Table 3 above.

Referring back to Fig. 7 , the probable wavelength and, hence, overall efficiency can be estimated. Both from a resonance argument and from prior observations[12] on lower pressure mixtures, the probable reaction products from (26) can be identified as $N_2^+(B^2\Sigma_u^+)$. The most probable transition is the (0,1) vibrational component of the B→X transition at 4278 Å. This corresponds to a 2.90 eV photon or an equivalent absolute quantum efficiency relative to the He^+ ion at 24.5 eV of 11.8%. This value together with expression (21) for the efficiency for the production of He^+ gives an overall efficiency Eff(λ) of

$$\text{Eff. } (4278\ \text{Å}) = 6.8\% \quad , \tag{27}$$

assuming reaction (43) goes to completion so that one photon per ion is realized.

From the above considerations, it appears peak power densities of the order of a Gigawatt per liter should be available to potential laser transitions for reasonable values of experimental parameters, provided the requisite population inversions occur. Considering only the better known N_2^+ system, the Einstein B-coefficient for absorption and stimulated emission can be written[16] as

$$B = \frac{1}{8\pi hc\nu^3} \quad \frac{g_n}{g_m} \quad \frac{1}{\tau} \tag{28}$$

where it is assumed the upper state is n and the lower, m; ν is in cm^{-1} and the g's are degeneracies, and for the $N_2^+(^2\Sigma_u^+ \rightarrow {}^2\Sigma_g^+)$, τ, the lifetime for spontaneous emission, is[17]

$$\tau = 66 \text{ nsec} \quad . \tag{29}$$

The expression for the amplification or absorption of radiation for an optical path length Δx in these units is[16]

$$\Delta I = I_o \cdot \Delta x \frac{Bh\nu}{\Delta\nu} \quad \frac{g_m}{g_n} \quad N_n \left(1 - \frac{g_n}{g_m} \frac{N_m}{N_n}\right) \quad , \tag{30}$$

where ΔI is positive for amplification, $\Delta\nu$ is the bandwidth of the initial radiation, and I_o and ΔI are the intensity and intensity increment, respectively. Defining a gain coefficient, K_o, evaluated at the center of the emission line so that the growth of intensity through the medium is

$$\Delta I = I_o R \kappa_o \Delta x \quad , \qquad (31)$$

where

$$R = \begin{cases} \dfrac{\Delta\lambda o}{\Delta\lambda} & \text{if } \Delta\lambda \geq \Delta\lambda o \\ 1 & \text{otherwise} \end{cases} ,$$

gives as a result of substituting (28) into (30) ,

$$\kappa_o = \frac{\lambda^2}{8\pi c \Delta\nu_o} \frac{1}{\tau} N_n \left(1 - \frac{g_n}{g_m} \frac{N_m}{N_n}\right) \quad . \qquad (32)$$

This expression must be corrected to reflect the molecular structure of the transition by replacing τ with the inverse of the A-coefficient times the Franck - Condon factor, $f^+(\nu',\nu'')$ and by replacing the population of the upper state with the fraction of population in the most populated rotational component

$$N_n(Jmax) = \frac{2J_m+1}{Z_r} \; N_n \quad , \tag{33}$$

where Z_r is the rotational partition function[18]

$$Z_r = \frac{\kappa T}{hcB_\nu} \quad , \tag{34}$$

and κT is the average rotational energy and B_ν is the spacing parameter for rotational levels. For the B-X band $J_m \sim 8$ and from tabulated[19,20] spectroscopic constants $(2J_{m+1})/Z_r = .134$, and $f^+(0,0)A = 1.24 \times 10^7$, $f^+(0,1)A = 2.20 \times 10^6$, $f^+(0,2)A = 5.01 \times 10^5$, and $f^+(0,3)A = 1.05 \times 10^5$ sec^{-1}.

To evaluate expression (32) for the various experimental conditions requires an assumption about the branching ratio for the yield of reaction (26). A lower limit can be obtained for the gain by ignoring the resonant nature of the excitation which favors the upper $B^2\Sigma_u^+$ state and assuming equal partition into the upper B and lower $X^2\Sigma_g^+$ states with the distribution among vibrational levels proportional to the Franck-Condon factors from the ground state of N_2 to the B and X states of the ion.

Collecting terms (32) becomes

$$\kappa_o \max(\nu', \nu'') = \frac{\lambda^2}{8\pi c \Delta\nu_o} \; Af^+(\nu',\nu'') \; (1-e^{-1}) \; X$$

$$\frac{1}{2} \; \frac{(2J_{m+1})}{Z_r} \; N_e f^B(\nu',0) \; \left(1 - \frac{g_n}{g_m} \; \frac{f^X(\nu'',0)}{f^B(\nu'',0)}\right) \tag{35}$$

where N_e is the initial charge density. Values for f^B and f^X are given by Nicholls.[20]

Then, provided the lifetime for charge transfer into the states as shown in Table 3 is significantly less than the natural radiative lifetime of 66 nsec., the information from Table 2 can be used with expression (35) to give the expected small signal gain per cm. In this evaluation, the linewidth $(\Delta\lambda o)^{-1}$ has been set to 1 cm^{-1} to facilitate scaling by the unknown pressure-broadened linewidth, and resulting entries in Table 4 should be reduced by the actual linewidth in cm^{-1}. Values resulting from (35) have been halved to account for the nearly equal division of line strength between P and R branches of the spectrum.

TABLE 4

Expected gain coefficients for the He:N_2 plasmas parameterized in Table 2 for 20 KA excitation. Gains should be scaled by the inverse pressure--broadened linewidth $(\Delta\lambda o)^{-1}$ in cm^{-1}.

Wavelength	3914 Å	4278 Å	4709 Å	5228 Å
(ν',ν'')	(0,0)	(0,1)	(0,2)	(0,3)
Helium Pressure (Atm)				
3	-.0038	.057	.018	.0045
30	-.038	.57	.18	.045

Even in the low pressure case, the gains are high enough after the reduction in the tabulated values because of the pressure broadening to permit the extraction of stimulated emission from the plasma. Thus, the elements of the theory are sufficient to show that charge transfer reactions should provide useful laser pumping mechanisms.

The results of Table 4 indicate that, at some time after the onset of the growth of ionization in the electron beam produced plasma, the threshold for lasing can be satisfied for a cavity of practical characteristics. At that point, it can be expected the cavity will oscillate, and the resulting stimulated emission will dump as laser radiation the stored energy corresponding to the fraction of He^+ converted to N_2^+ B state molecules by that time. From Table 2 it can be seen that this output energy could be as large as 73 Joules/liter at 100 KA and 30 atm and could represent 6.8% of the energy lost by the beam in the radiating volume. However, this assumes the gas mixture can be perfectly optimized. In practice, the filling of the lower $X^2\Sigma_g^+$ states by spontaneous emission, unfavorable branching and chemical and electrical quenching of the B state will determine a maximum effective time, τ_M, over which the charging function can be integrated to yield stored energy which can be recovered with the modelled efficiency. Because of the paucity of data describing these limiting effects, further refinement of the model to derive τ_M is unwarranted at this time. Rather, the results of parameterization of the phenomenology of test laser devices pumped by this charge transfer mechanism can serve to provide the characterizing data needed to complete the model.

However, it is important to recognize that the potentially limiting mechanisms are minimized in the charge transfer scheme described here. In this fact lies the primary advantage in this mechanism. It results primarily from the large cross sections[14], 10^{-14} cm^2, characteristic of such processes. This is to be compared with the value of 0.05×10^{-14} cm^2 characteristic of the argon-nitrogen reaction recently reported[19] to lead to laser emission in argon-nitrogen mixtures. These values for the charge transfer process are at least an order of magnitude larger than those characteristic of most excitation

transfer reactions involving neutral atomic and molecular species. This means much smaller concentrations of the gas to be excited can be used which, in turn, means that chemical quenching of the final excited state population should be virtually negligible, as seems to be the case in the nitrogen ion laser finally realized.

III. GAIN MEASUREMFNTS

The entry point into the problem of evaluating the utility of charge transfer reactions as laser pumping mechanisms in plasmas excited by an e-beam discharge was felt to be in the acquisition and identification of the spontaneous emission from the proposed system. Because of its availability at the time, a Febetron 706 electron-beam device discharging single pulses of 500 KeV electrons of 3-nsec duration into a gas mixture of 3 atm of helium and a few Torr of nitrogen was used for spectroscopic observations of the resulting afterglows. The test gas was contained in a rectangular cell fitted with sapphire viewing windows to permit probing of a lamina of plasma transverse to and excited by primary electrons which penetrated equal distances into the cell. The optical axis was terminated on one side of the plasma by a dielectric mirror to provide in later experiments for the return of a probing laser beam.

The resulting spectrum is shown in Fig. 8 for the cases of an e-beam discharge into two samples of nitrogen, 4.9 Torr and 42.4 Torr, diluted in 3 atmospheres of helium. For the lower partial pressure of nitrogen, the spectrum shows the strong selective excitation of the $B^2\Sigma_u^+ \rightarrow X\ ^2\Sigma_g^+$ transitions of N_2^+, as expected on the basis of the discussion of Section II. Conversely, the higher partial pressure exceeds the limits set in Table 4 for a "clean" charge transfer reaction system from primary He^+ to secondary He_2^+ to $N_2^+(B^2\Sigma_u^+)$. In agreement with those expectations, intensities in the high pressure case are reduced, and there is a partition of the energy into the Second Positive band system of the neutral N_2 indicating a much more complex reaction chain.

Figure 8

Survey Spectrum of the visible region made using an f/2 spectrograph. Long wavelengths are to the right. The upper spectrum for a gas mixture of 3 atmospheres of helium and 4.9 Torr N_2 shows strong selective excitation of the First Negative system of N_2^+ as expected from the discussion in Section II. The lower spectrum at the same helium pressure but a higher N_2 partial pressure (42.4 Torr) shows a considerable reduction in overall intensity and the appearance of second positive band system of the neutral N_2. As shown in Table 3, this latter case exceeds the N_2 pressure limits set for a "clean" charge transfer reaction system.

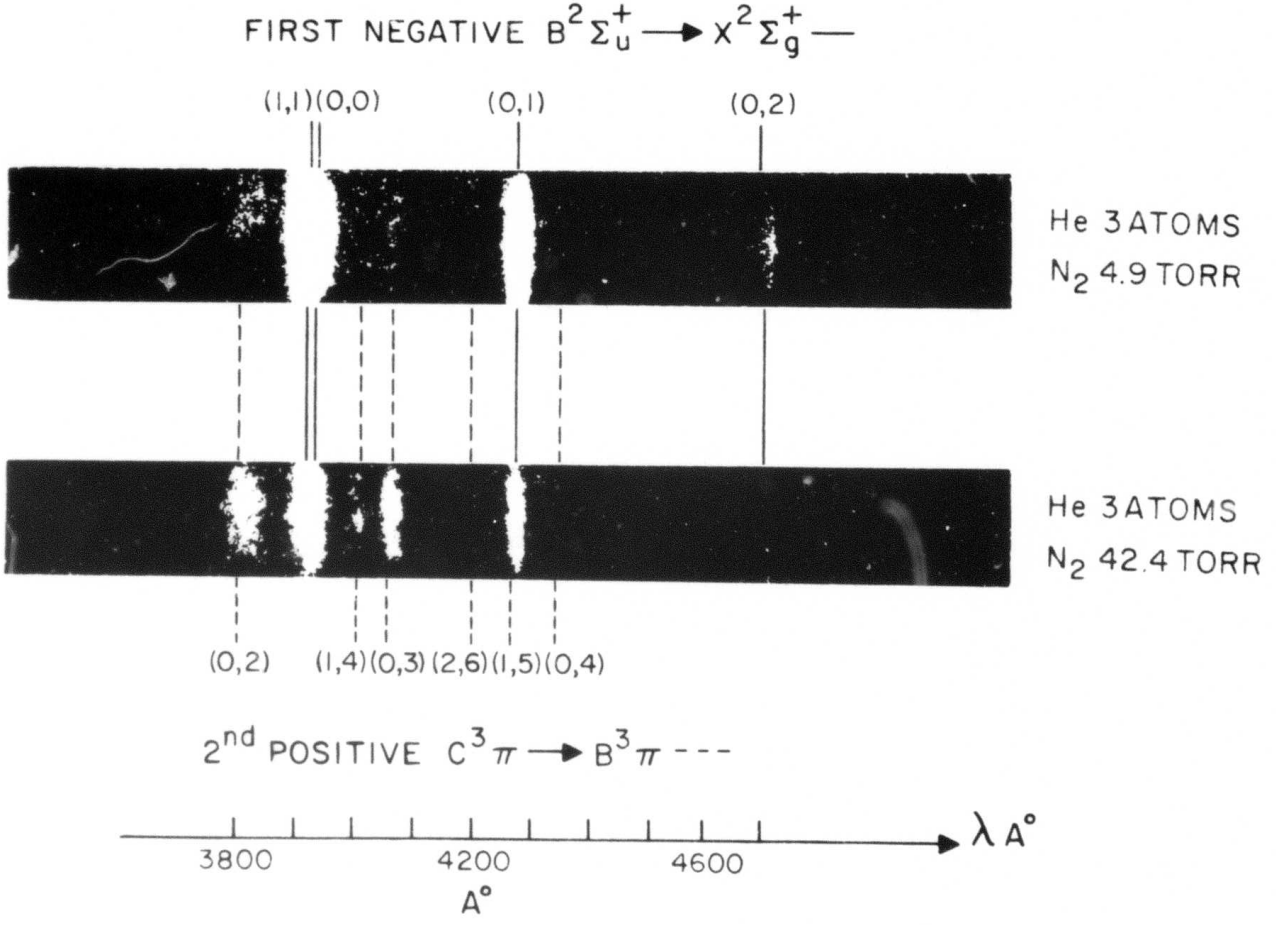
FIRST NEGATIVE $B^2\Sigma_u^+ \longrightarrow X^2\Sigma_g^+$
(1,1)(0,0)
(0,1)
(0,2)
He 3ATOMS
N_2 4.9 TORR
He 3ATOMS
N_2 42.4 TORR
(0,2)
(1,4)(0,3)(2,6)(1,5)(0,4)
2nd POSITIVE $C^3\pi \longrightarrow B^3\pi$
3800
4200
4600
λ A°
A°

A quantitative system for the direct measurement of gain was constructed as shown in Figure 9. Since the lifetimes for the source of molecular emissions were generally less than 100 nsec as discussed in Section II, it was necessary to use a rapidly pulsed light source for the measurement of small signal gain or absorption in a particular transition during the afterglow period. A nitrogen laser pumped, tunable dye laser with a FWHM of a few Angstroms was used in the differential path arrangement shown in Fig. 9 to measure the attenuation or amplification of the beam reflected through the plasma by the internal dielectric mirror. Use of the optical delay line in the reference path allowed for the detection of both beams with a single photomultiplier and electronics system thus minimizing the drift of the balance of sensitivity between the paths. Resulting system stability was of the order of 6% with timing jitter between the e-beam and the dye laser small in comparison with a reaction lifetime. As accuracy of the timing measurement was around 4 nsec., adequate resolution of the particular phase of the plasma sampled by the dye laser beam could be established.

These measurements also were conducted on plasmas excited by the Febetron 706 at two current levels computed to be around 0.6 KA/cm^2 and 2.0 KA/cm^2 when the divergence of the beam and the distance to the foil window were considered. In the case of the lower current excitation, Fig. 10 shows the topology of the map of gain resulting from the measurements over the t, λ space of parameters as indicated. For each of the different vibrational transitions examined, substantial small-signal gains were recorded in both the P-branches containing the band heads and the R-branches trailing to shorter wavelengths. Units plotted are the fractional gain per

Figure 9

Experimental system for the direct measurement of gain spectra.

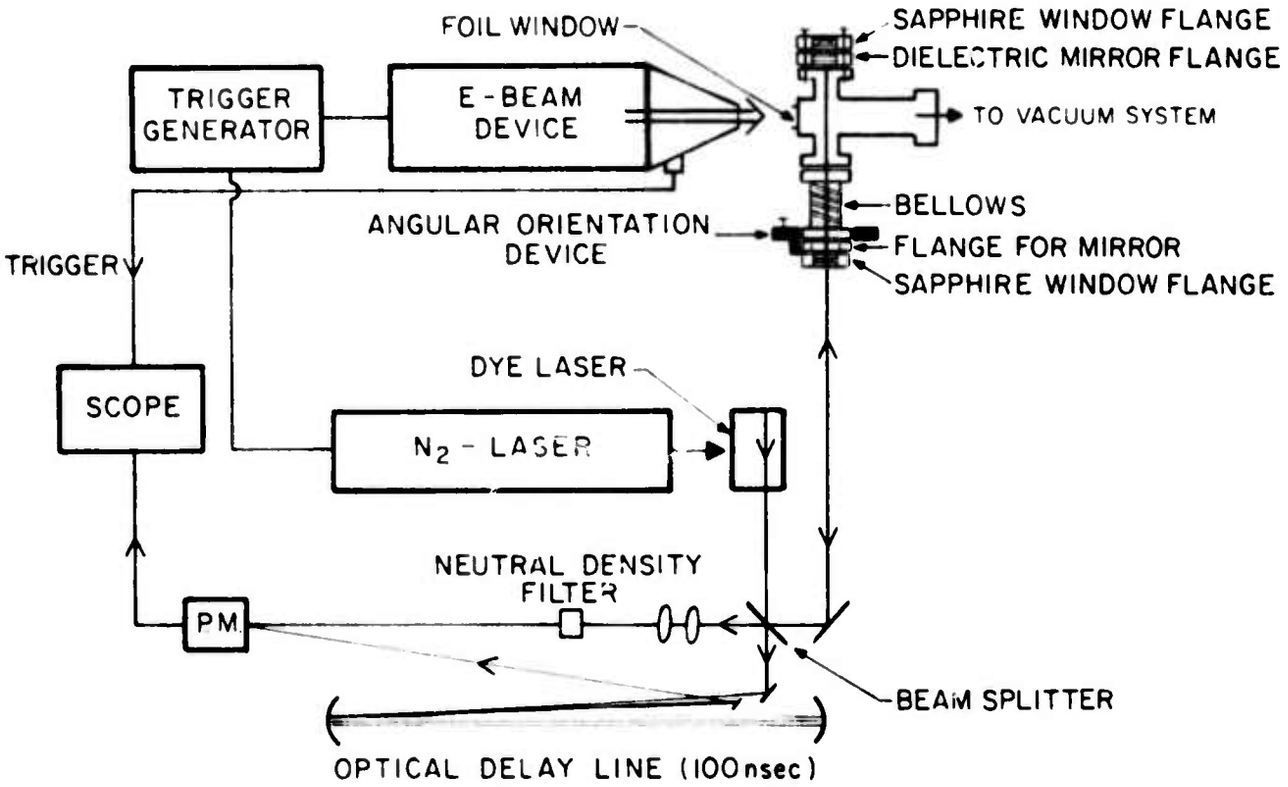
FOIL WINDOW
SAPPHIRE WINDOW FLANGE
DIELECTRIC MIRROR FLANGE
TRIGGER GENERATOR
E-BEAM DEVICE
TO VACUUM SYSTEM
BELLOWS
ANGULAR ORIENTATION DEVICE
FLANGE FOR MIRROR
TRIGGER
SAPPHIRE WINDOW FLANGE
DYE LASER
SCOPE
N_2 - LASER
NEUTRAL DENSITY FILTER
PM
BEAM SPLITTER
OPTICAL DELAY LINE (100nsec)

Figure 10

Fractional gain per round-trip transit of the plasma as a function of wavelength and time for the afterglow of an electron-beam discharge into 3 atm of helium containing 0.8 Torr nitrogen. Regions of stimulated emission lie above the t,λ plane; absorption below. Across the t,z plane to the rear of the data has been plotted the common time dependence of the spontaneous emission for scale. On the λ,z plane to the left edge is shown the normal spontaneous emission spectrum of the N_2^+ 1st negative bands of the $B^2\Sigma_u^+ \rightarrow X^2\Sigma_g^+$ transition, uncorrected for broadening mechanisms. The corresponding vibrational states (v',v") of the upper and lower electronic states, respectively, are shown in parentheses.

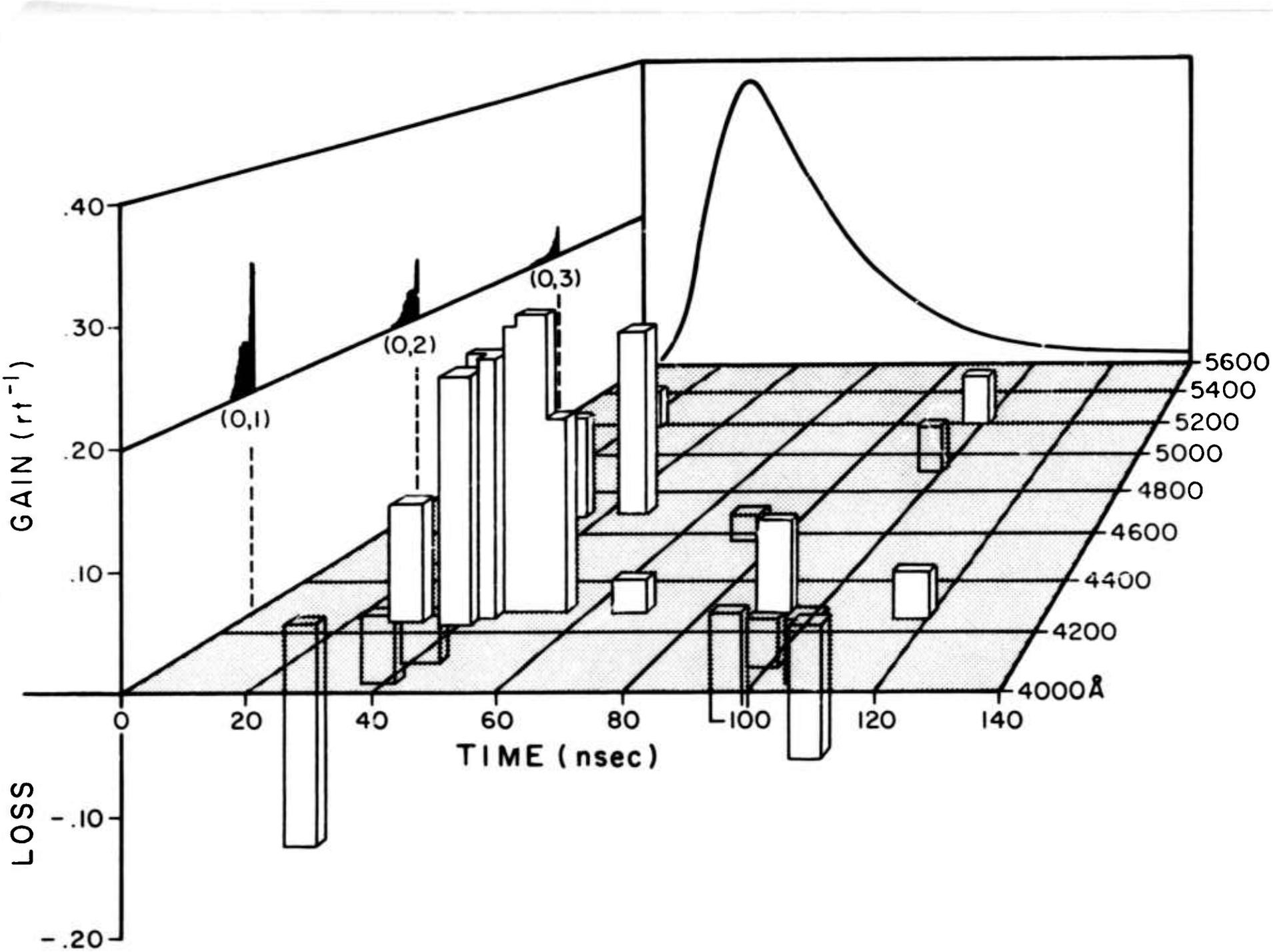
.40
.30
.20
.10
GAIN (rt⁻¹)
(0,1)
(0,2)
(0,3)
5600
5400
5200
5000
4800
4600
4400
4200
4000Å
0
20
40
60
80
100
120
140
TIME (nsec)
LOSS
-.10
-.20

round-trip transit of the afterglow. The peak gain of 0.30 seen at 50 nsec in the 4278 Å transition corresponds to a gain coefficient of 0.05 cm^{-1}.

As can be seen in the figure, and in greater detail in the section at 4278 Å shown in Figure 11, however, the temporal evolution of the gain coefficient was found not to be simply proportional to the upper state population as evidenced in comparison to the spontaneous emission profile shown. Later peaking of the gain suggests relaxation to the v'=0 level of some of the population of the higher vibrational states initially produced by the charge-transfer reaction (26). The same general dependence, but with decreasing amplitude was found for the (0,2) and (0,3) bands at 4709 and 5228 Å, respectively. Although data for times preceding the gain peak were quite sensitive to the precise gas composition and initial discharge current density, the occurrence and time decay of the gain were not.

Further confirmation of the magnitude of the gain was obtained from observation of the axial intensity emitted from a resonant cavity containing the plasma as a function of cavity length[22]. Cavity amplifiers were used in which the mean lifetime of a photon in the cavity considerably exceeded the lifetime of the amplifying medium. For these measurements, the dye laser was removed, and a dielectric mirror of 99% reflectance at 4278 Å was added. Optics were used having solid angles of acceptance small compared to the solid angle spanned by the forward lobe of the radiation pattern from the cavity. Under these conditions, there is no geometric effect, and the axial intensity is simply a function of the number of transits of the plasma a photon can make before the plasma decays and the

Figure 11

Time evolution of fractional gain (loss) per round trip transit of the plasma for the 4278 Å (0,1) first negative transition of N_2^+ in the afterglow of an electron beam discharge into 3 atmospheres of helium containing 0.8 Torr nitrogen.

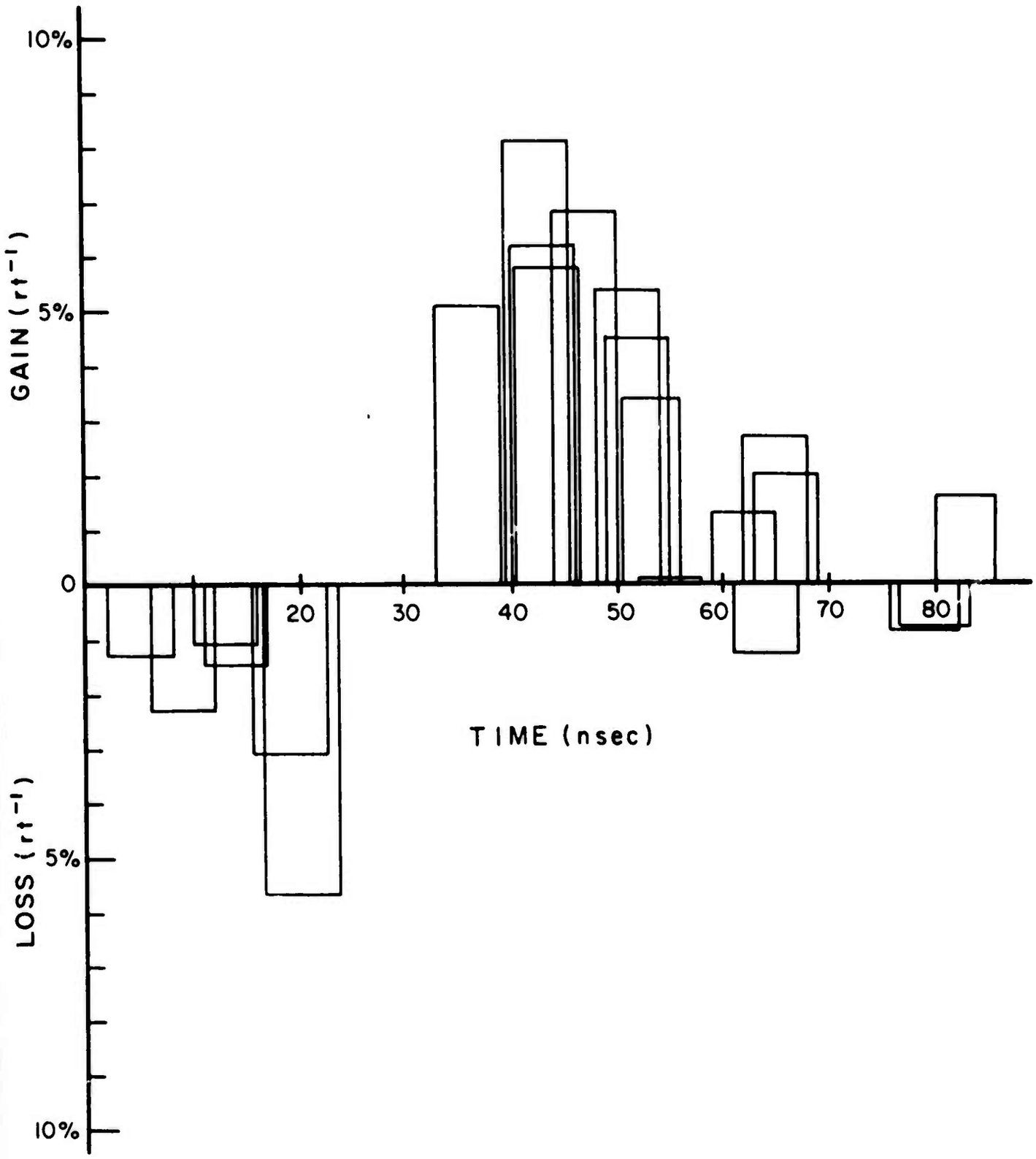
4278 Å (0,1)
10%
5%
0
5%
10%
GAIN (rt⁻¹)
LOSS (rt⁻¹)
20
30
40
50
60
70
80
TIME (nsec)

average gain or loss occurs during each transit.

Fig. 12 summarizes the resulting energy per pulse emitted axially at 4278 Å and normalized to the isotropic incoherent emission from the afterglow for cavities of four different lengths. The passive loss of the cavity was determined to be 3% per round trip from the exponential decay of the axial intensity following the termination of the afterglow. The slope of the curve of Fig. 11 is related to average net gain over the lifetime of the plasma[22], and the value of 0.02 cm^{-1} obtained is less than the peak gain seen in Fig.10 as would be expected from the larger bandwidth of the interference filter isolating the axial emission at 4278 Å.

The measurements represented the first demonstration of the potential utility to high energy laser development of charge transfer reactions as e-beam laser pumping mechanisms and were reported in Applied Physics Letters[1]. The subsequent construction of the first nitrogen ion laser pumped by this charge transfer reaction is reported in the following section.

Figure 12

Functional dependence on the number of round-trip transits of the cavity made by a photon during the 60-nsec lifetime of the spontaneous emission of the energy emitted axially per pulse from a resonant cavity enclosing the plasma. Each measurement is normalized to the energy of the spontaneous incoherent radiation emitted at the same wavelength selected by an interference filter centered at 4264 Å with a FWHM of 57 Å.

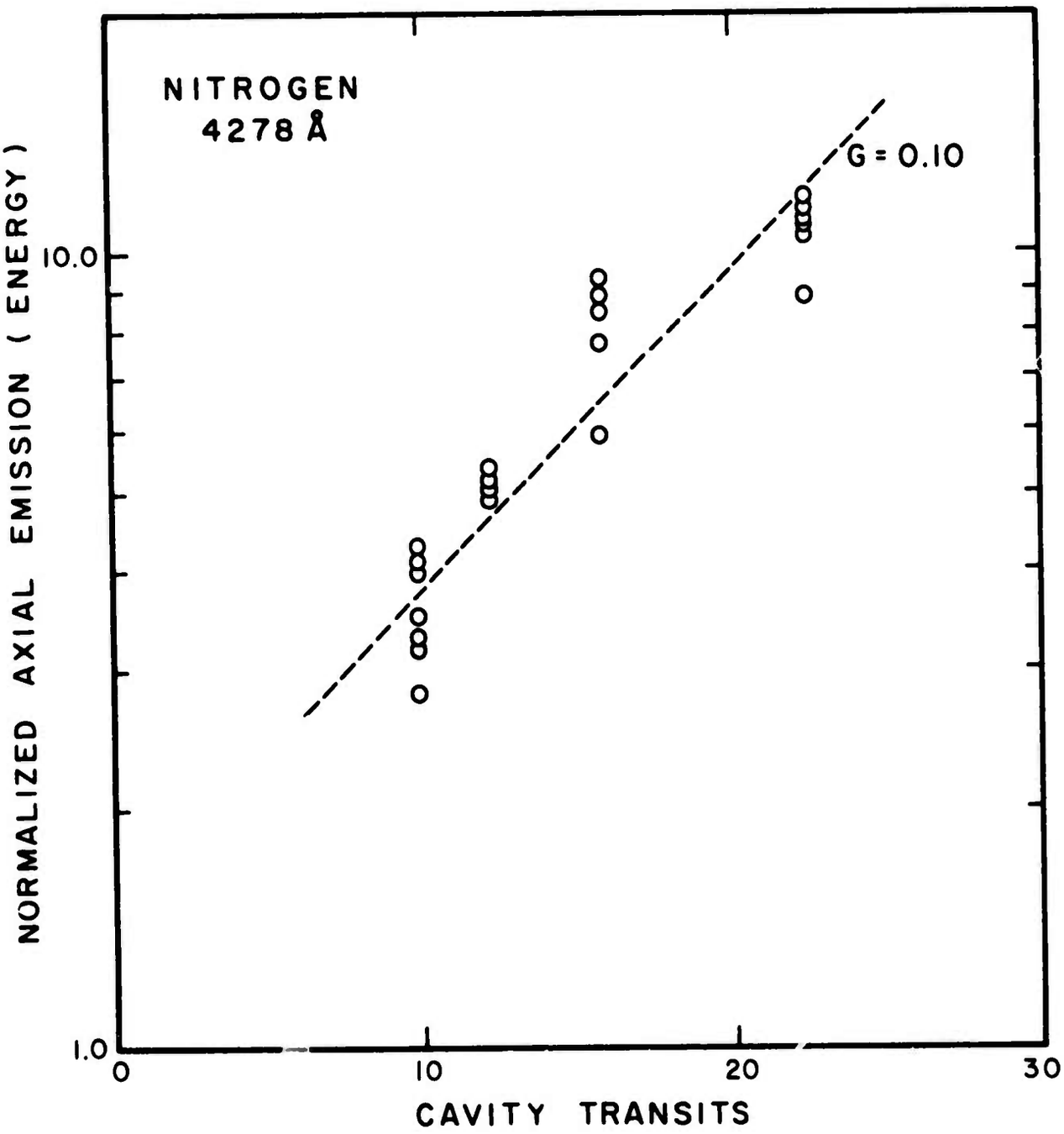
NITROGEN
4278 Å
G = 0.10
NORMALIZED AXIAL EMISSION (ENERGY)
10.0
1.0
0
10
20
30
CAVITY TRANSITS

IV. THE NITROGEN ION LASER, INITIAL CHARACTERIZATION

The initial series of experiments described in this section were conducted on APEX-1, the 100 KA, 1 MeV device discussed in Section II, at the manufacturer's facility prior to acceptance of the device. Preliminary results were reported in a Special Technical Report[10] and subsequent letter[2]. This experimental series was necessarily of a limited scope and designed to verify the theoretical predictions, confirmed by subsequent gain measurements, that the charge transfer reaction

$$He_2^+ + N_2 \rightarrow N_2^+(B^2\Sigma_u) + 2\ He \qquad (36)$$

held important promise as a laser pumping mechanism. In this regard, the experiments were completely successful.

The APEX-1 electron beam gun was constructed by Systems, Science and Software of Hayward, California. The device is a fast pulse, sheet beam gun emitting 100 KA pulses of 1 MeV of 1 x 10 cm transverse cross section. Pulse durations are typically 20 nanosecond FWHM with a 6.6 nanosecond rise time and a fall time controlled by a shorting electrode. By proper adjustment, the fall time can be reduced to less than 7 nsec. During the experimental series reported here, the anode-cathod[illegible]ng in the output diode was increased to give a larger diode impedance and consequent peak current of 13.4 KA. Larger currents were not attempted as the operation under those conditions had not been established at that time.

The afterglow chamber used in these e-beam laser experiments was necessarily different from the HPAC series[23] developed under this contract for use with the Febetron 706. The new e-beam laser afterglow chamber (ELAC-1) consisted of a laser cavity mounted to a foil support assembly and contained in a cylindrical high pressure vessel with axis of symmetry along the axis of beam propagation as shown in Figure 13. The assembly was constructed of UHV-grade stainless steel with windows and gas handling connections

Figure 13

Exploded view of the e-beam laser afterglow chamber (ELAC-1) operated as the first nitrogen ion laser.

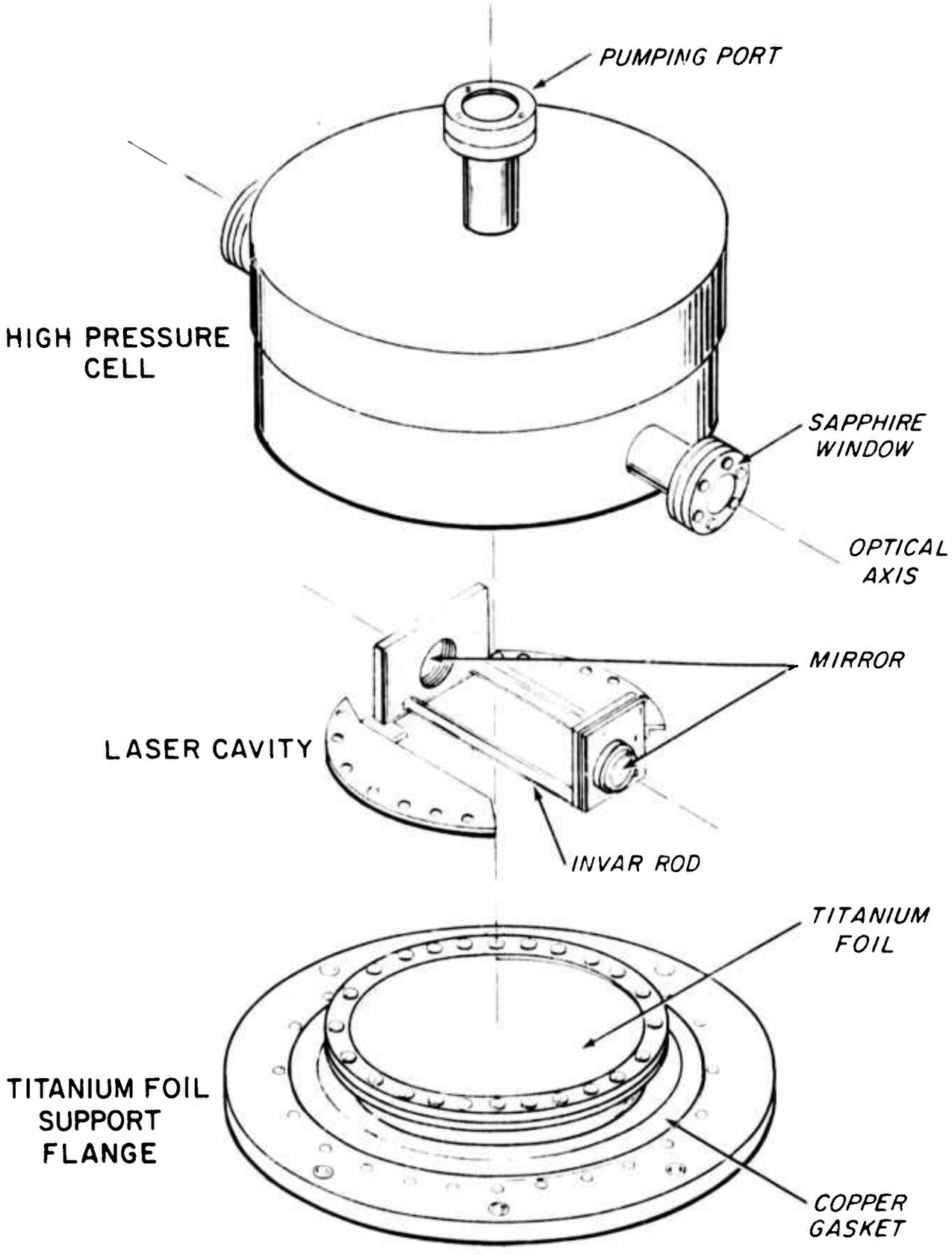
PUMPING PORT
HIGH PRESSURE CELL
SAPPHIRE WINDOW
OPTICAL AXIS
MIRROR
LASER CAVITY
INVAR ROD
TITANIUM FOIL
TITANIUM FOIL SUPPORT FLANGE
COPPER GASKET

made with Varian-type copper shear seals. The laser cavity consisted of a pair of 1 m. dielectric mirrors which were mounted to allow angular alignment, spaced with 14 cm invar rods, and contained in the pressure vessel with sapphire windows sealed across the optical axis external to the cavity as shown in Figure 13.

In operation the system was pressurized with 7 atmospheres of a mixture of helium and nitrogen. Useful partial pressures of nitrogen ranged from 2 to 20 Torr. Excitation was provided by the electron beam from APEX entering through a supported, 0.002-in. thick titanium foil window and propagating in a direction perpendicular to the optical axis.

Spectra were first recorded with a scope camera focused on the image plane of a 0.25 m Jarrell Ash spectrometer with exit slit removed. Resolution was limited to 3 Å by the 100μ width of the entrance slit and the dispersion of the grating. The time dependence and power level of the light output was measured with a calibrated ITT F-4000, S20 vacuum photodiode connected directly to a Tektronix 519 oscilloscope. Proper attenuation of the laser output was provided by calibrated neutral density filters.

In operation, an intense violet emission from the laser could be seen on a white card placed to intersect the optical axis after it emerged from the pressure vessel. Typical operation is recorded in Fig. 14 where the white card has been replaced by a ruled translucent screen. The elliptical shape of the output spot is a result of masking of the beam by an off-axis obstruction erroneously introduced into the pressure vessel. Beam divergence was measured to be 20 milliradians from photographs of the illuminated spot on such targets successively placed at distances varying from 1 to 10 m.

Examination of the spectrum of the laser emission showed the single line

Figure 14

Emission from the first nitrogen ion laser. The output beam is seen in the photograph striking the ruled translucent target in the lower left. The emission consists of a single spectral line of less than 3 Å linewidth at 427 nm in the violet. The laser cavity is contained in the pressure vessel with sapphire windows sealed across the optical axis.

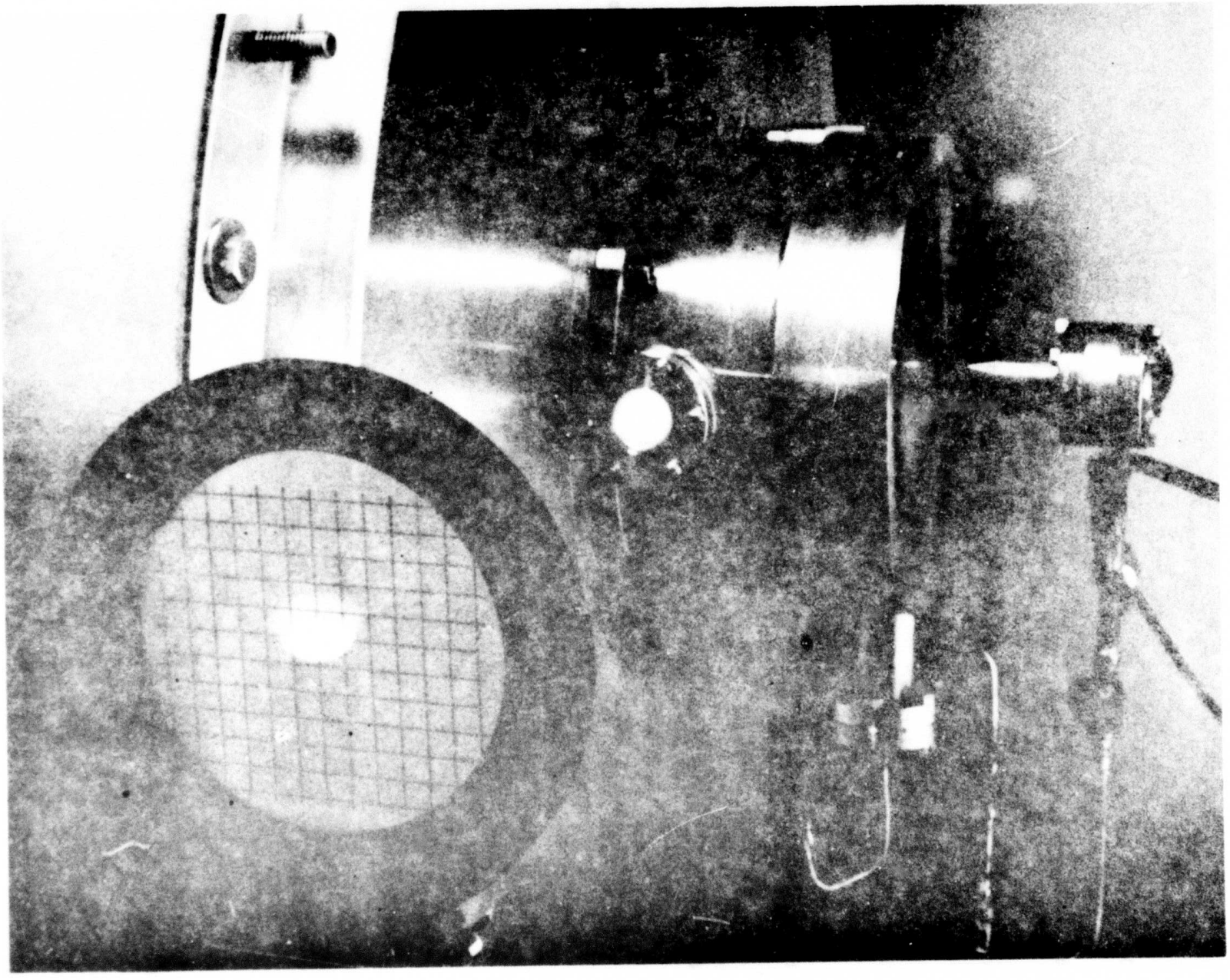

at 4278 Å. This line corresponds to the band head in the P-branch of the (0,1) vibrational transition of the $B^2\Sigma_u^+ \rightarrow X^2\Sigma_g^+$ electronic transition of the nitrogen molecular ion, N_2^+. The width on the original film of the laser emission line corresponded precisely to the 0.1 mm physical width of the entrance slit and established the laser line width to be $\Delta\lambda < 3$ Å.

The radiating volume was estimated to be 0.625 cm^3 from application of a double cone geometry to enlarged photographs of the illuminated spot at the base of the cone on the output dielectric mirror.

A typical time-resolved power measurement is shown in Fig. 15 together with a recording of beam current plus an additive L di/dt artifact. The peak laser power shown is 9.1 KW and therefore corresponds to an emitted energy density of 0.22 J/liter. The decay of the pulse can be seen to correspond to the ringing down time of the cavity and indicates that the total energy of the output pulse is extracted prior to the pulse maximum around 11 nsec. The energy lost by the beam during the corresponding first 11 nsec can be obtained by integrating the ionizing function F(E) shown in Fig. 6. However, since the integration limit $t \sim 11$ nsec lies in the domain $t > \tau$, eq (16) can be used.

Fig. 16 shows an enlarged representation of the timing relevant to the determination of the energy deposition from the beam. The dashed curve

Figure 15

Upper trace - Time resolved power measurement of the laser output at 10 Torr partial pressure of N_2 from a 14 cm cavity having 8.8% loss per round trip transit. Peak power corresponds to 9.1 KW. The horizontal scale is 15.8 nsec/div.

Lower trace - Time resolved record of the total electron beam current collected with a Faraday cup. Peak current density corresponds to 1.4 KA/cm^2 at 1 MV.

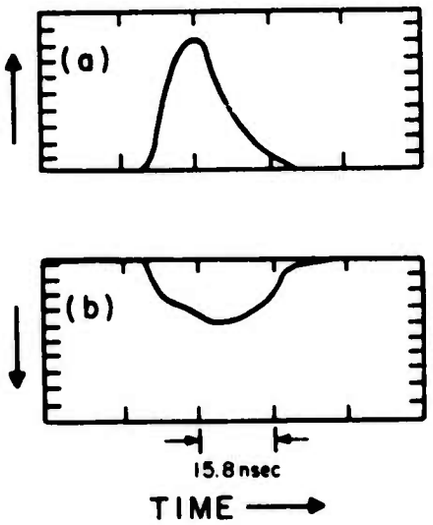

(a) Radiated Intensity
(b) Beam Current

Figure 16

Graphs as functions of time of the electron beam current, the corresponding calculated energy deposition and the laser output power. The dashed curve represents a linear approximation to the beam current used in the energy deposition calculations. The ordinate scale is common to all curves, and units for each are as marked.

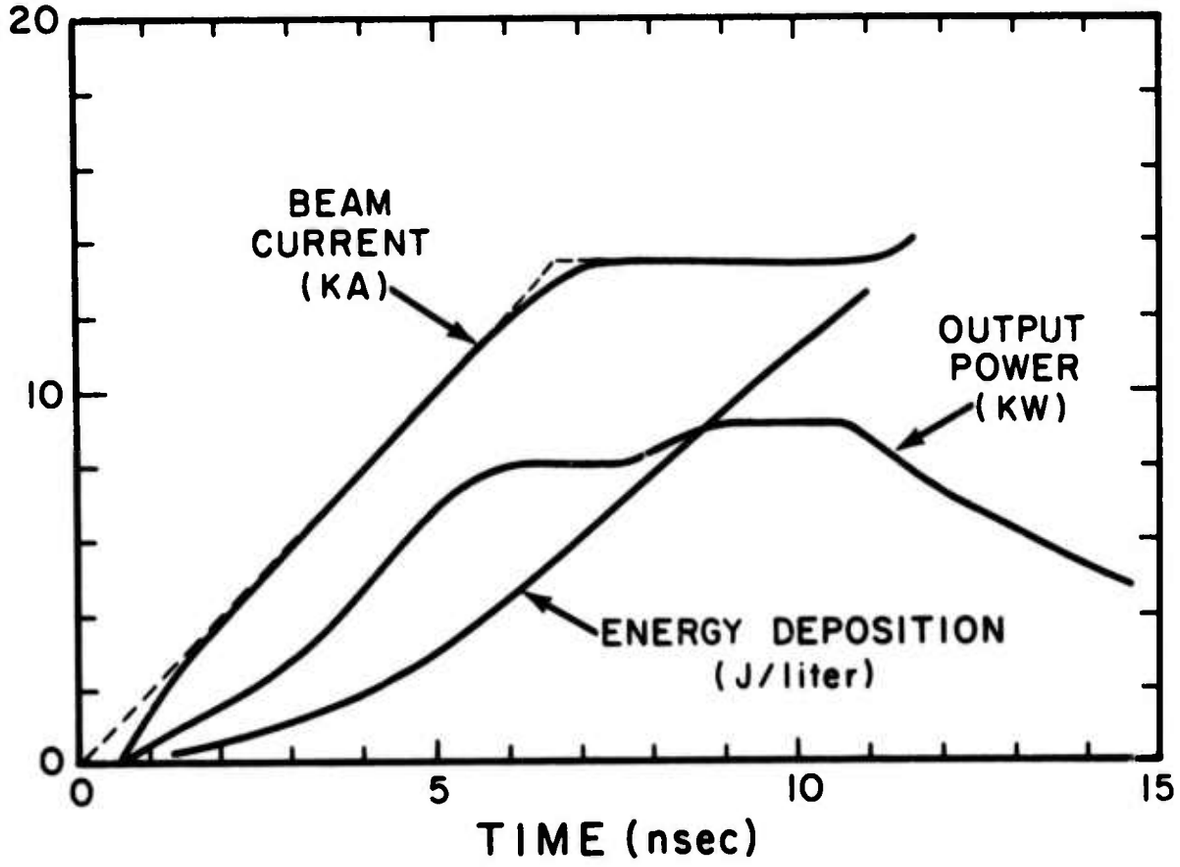
20
10
0
0
5
10
15
TIME (nsec)
BEAM
CURRENT
(KA)
OUTPUT
POWER
(KW)
ENERGY DEPOSITION
(J/liter)

represents the fit to a linear risetime used in the calculations of energy deposition. It is consistent with the sharper onset of the measured beam current seen in the figure and expected from the calculations presented in Figure 5. It appears that the "ringing down" of the output laser pulse begins about 10.8 nsec, and this time should be used in eq (16) as discussed above, to estimate the energy deposition from the beam. In this case, then,

$$\varepsilon = 12.4 \text{ Joules/liter.} \tag{37}$$

This gives an output efficiency for 427 nm radiation of 1.8% relative to the energy lost in the radiative volume. This is to be compared with the theoretical limit of 6% for delta function, e-beam excitation at a time early enough for reaction (36) to go to completion.

As mentioned in Section II, the relevant scaling of gain for different lower state vibration components from the same v=0 upper state of the B → X transition should be roughly proportional to the product $Af^{+}(0, v'')$, where v" is the vibrational quantum number of the lower state. From the tabulation of constants following eq (34), it can be seen that the gains for the 427, 471 and 523 nm transitions corresponding to v"=1, 2 and 3, respectively, should be in the ratio 21: 4.8: 1. Since lasing at 427 was accomplished with as much as 20% mirror loss per round trip, it should have been possible to force oscillation at 471 and 523 nm with suitable mirrors of not unrealistic characteristics.

A very brief attempt to obtain laser emission at 471 was made at the end of the experimental sequence. Using a mirror set with 36% loss per round trip at 427 nm and 1.5% at 471 nm, laser emission was observed to have a pronounced blue color. Photographs of the spot formed on a transulcent screen

made with and without interference filter peaked at 427 nm showed the laser output to be blocked by the 427 nm filter. Limitations on time and available optics prevented further experimentation along these lines, but it appears *a priori* that laser output at 471 has been observed. Coatings more appropriate for the purpose will be needed for future investigation and optimization of 471 nm and perhaps 523 nm emission.

V. THE NITROGEN ION LASER, SCALING CONSIDERATIONS

Following acceptance testing of APEX-1 at the Dallas facility, a second experimental series was begun for the purpose of verifying the scalability of the nitrogen ion laser system. This series is currently in progress and preliminary results are reported in this section.

The relatively high efficiencies reported in the previous section were clearly contingent upon both the accuracy of the measurement of the volume from which energy was extracted, as well as whether or not this was a representative volume. As concave mirrors were used to bound the plasma volume, several difficulties were present. The fact that the lifetime of the amplifying medium was short compared to the lifetime of a photon in the cavity meant the mode configurations characteristic of stable resonators were not appropriate. The actual configuration operated more as an "optical delay line" composed of concave mirrors. Ray tracing suggested successive focusing and defocusing of the beam upon successive reflections so that some transits of the plasma occurred with a large beam diameter and some with a very small one. Since the gain of the medium was time dependent, each transit occurred not only with a different geometry, but with a different effective gain parameter.

To avoid the difficulties a plane mirror set was procured. The rear mirror was totally reflecting and the output mirror transmitted 8% of the incident beam at 4278 Å. Unfortunately, this particular mirror set also had a reasonably high-Q at the 3914 Å wavelength region corresponding to the (0,0) vibrational component of the same electronic transition.

This plane mirror set was used in the same ELAC-1 apparatus shown in Figure 13 of the previous section. The mechanical obstruction was still present,

and restricted about half of the mirror area. The result was a free aperture for the laser output which was slightly elliptical. The resulting volume from which output energy was extracted had the form of an elliptic cylinder with ends slightly slanted at an angle of $\bar{\phi}$. The resulting volume was 25 cm^3 and the cross sectional area was confirmed from photographs of the illuminated area on the output mirrors. In this case there is no problem of focusing or defocusing of the beam and the total volume is large enough to be considered representative. As will be seen, divergence of the beam was small enough to suggest ignoring the reduction in volume caused by the narrowing of the lasing volume at the beam waist.

The resulting over-all characteristics of the laser output are summarized in comparison with the earlier results in Table 5.

Table 5

Comparison of Nitrogen Ion Laser
Characteristics for Concave and
Plane Mirror Sets

	Concave Mirrors	Plane Mirrors
Mode Volume	0.6 cm^3	25 cm^3
e-Beam Current	14 KA	14 KA
Beam Dimensions	1 x 10 cm	1 x 10 cm
Pressure (He)	7 Atm	7 Atm
(N2)	5 Torr	8 Torr
Spectral Linewidth	$\cdot$ 3 Å	$\cdot$ 0.3 Å
Beam Divergence	20 mR	3 mR
Peak Power	9 KW	75 KW
Pulse duration	15 nsec	10 nsec

Principal differences can be seen in the significant reduction in beam divergence which makes the value of mode volume much more certain in the plane mirror case. The change in the upper limit on spectral linewidth is simply a consequence of the better resolution available from the 0.75 m. Spex spectrograph used with 5 μ slits in the current experimental series.

The spectrum of the laser output is shown in Figure 17 together with a reference spectrum superimposed from a separate helium discharge lamp of 10^{10} times greater duty cycle. The laser line seen is identified on the reproduction and was found to have a wavelength of 4278 Å. It corresponds precisely with the band head in the P-branch of the (0,1) vibratic al component of the $B^2\Sigma_u^+ \rightarrow X^2\Sigma_g^+$ electronic transition of the nitrogen molecular ion N_2^+.

The power output can be seen to increase with volume although not in direct proportion to the apparent 40-fold increase in active volume. The discrepancy could be attributed entirely to inaccurracy in determining the volume in the case of the concave resonator were it not for the anomalous decrease in the duration of the laser pulse from 15 to 10 nanoseconds.

A closer examination of the spectrum showed that in the case of the plane mirrors the main laser pulse at 4278 Å was preceeded by a very short pulse at 3914 Å. The latter line corresponds to the (0,0) vibrational component of the same electronic transition as the 4278 Å line, and is shown in the spectrum reproduced in Figure 18. Since the two lines originate from the same upper state, the initial pulse of stimulated emission from the 3914 Å line would tend to deplete the upper state population and delay the time at which it exceeded the threshold for lasing the less probable 4278 Å transition. In this way the power output at 4278 Å could be both reduced and shortened by the precursive pulse from the (0,0) transition. This problem was not encountered with the original concave mirror set since its reflectiv was considerably less at the 3914 Å wavelength.

Figure 17

Spectrum of the nitrogen ion laser output. The single laser line is idenitfied on the spectrum and corresponds to the 4278 Å band head in the P branch of the (0,1) vibrational component of the $B^2\Sigma_u^+ \rightarrow X^2\Sigma_g^+$ electronic transition of the nitrogen molecular ion, N_2^+. Reference lines, identified below the spectrum, were superimposed from a separate helium discharge lamp of 10^{10} times greater duty cycle.

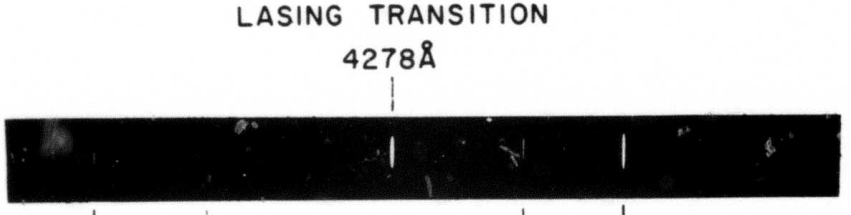

HELIUM REFERENCE SPECTRUM

Figure 18

Spectrum of the nitrogen ion laser output in the ultra-violet region. The laser line is indicated on the spectrum and corresponds to the 3914 Å band head in the P-branch of the (0,0) vibrational component of the $B^2\Sigma_u^+ \rightarrow X^2\Sigma_g^+$ electronic transition of the nitrogen molecular ion, N_2^+. Reference lines were superimposed from a separate helium discharge lamp of 10^{10} times greater duty cycle.

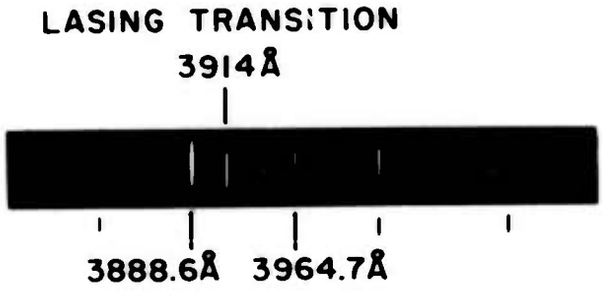

HELIUM REFERENCE SPECTRUM

To examine further the behavior of the 3914 Å laser pulse an ultraviolet mirror set was installed and the lower data set shown in Figure 19 was obtained. The output from the "normal" violet plane mirror cavity has been plotted for comparison. Both traces were recorded with a calibrated ITT F-4000, S20 vacuum photodiode connected directly to a Tektronix 519 oscilloscope. Proper attenuation of the laser output was provided by calibrated neutral density filters mounted to avoid the non-linear effects resulting from trapping of the intense beam between filters. The beam-sampling geometry was held constant in each case.

As can be seen, the 3914 Å component self-terminates in less than 2 nanoseconds and gives a measure of the time required for the lower laser state to "fill". Since the lower state of the 4278 Å differs only in vibrational quantum number, it has the same degeneracy and should "fill" to terminate the 4278 Å transition in a comparable time. That it does not, as seen in the figure, is strong evidence for the existence of an unblocking process tending to quench the vibrational excitation of the lower, $v''=1$, state of the 4278 Å transition. Further study is needed to characterize and optimize this process to extend the duration of the laser output.

It should be noted that the power plotted in Figure 19 is total power at all wavelengths and the precursive 3914 Å component can be seen in the upper data as the small "step" on the leading edge of the pulse. It can be seen to occur after the same delay from the beginning of the beam current as the total output in the lower trace. This precursive (0,0) component and its detrimental effect on output can be seen more clearly at lower partial pressures of nitrogen. The laser power output from the 4278 Å cavity is shown as a function of nitrogen partial pressure for a total pressure of 7 atmospheres in Figure 20. At the

Figure 19

Time resolved power measurements of the nitrogen-ion laser output for two different dielectric mirror sets optimized for the wavelengths shown to the right of each trace. Total power in all wavelengths is shown in each case. Total gas pressure was 7 atmospheres with a partial pressure of nitrogen of 7.5 Torr. The time scale is as indicated and has been shifted so that the zero corresponds to the beginning of the e-beam current output.

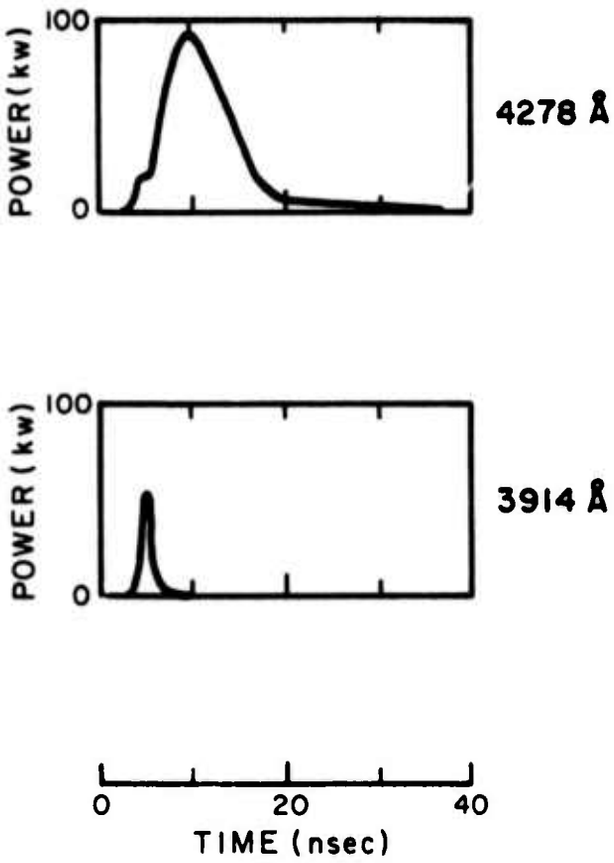
100
POWER (kw)
0
4278 Å
100
POWER (kw)
0
3914 Å
0
20
40
TIME (nsec)

Figure 20

Time resolved power measurements of the nitrogen-ion laser output from the optical cavity optimized for 4278 Å. Total gas pressure was 7 atm. with partial pressures of nitrogen shown to the right of each trace. The time scale is indicated below and has been zeroed to correspond to the initiation of the e-beam current. Peak e-beam current was 14 KA.

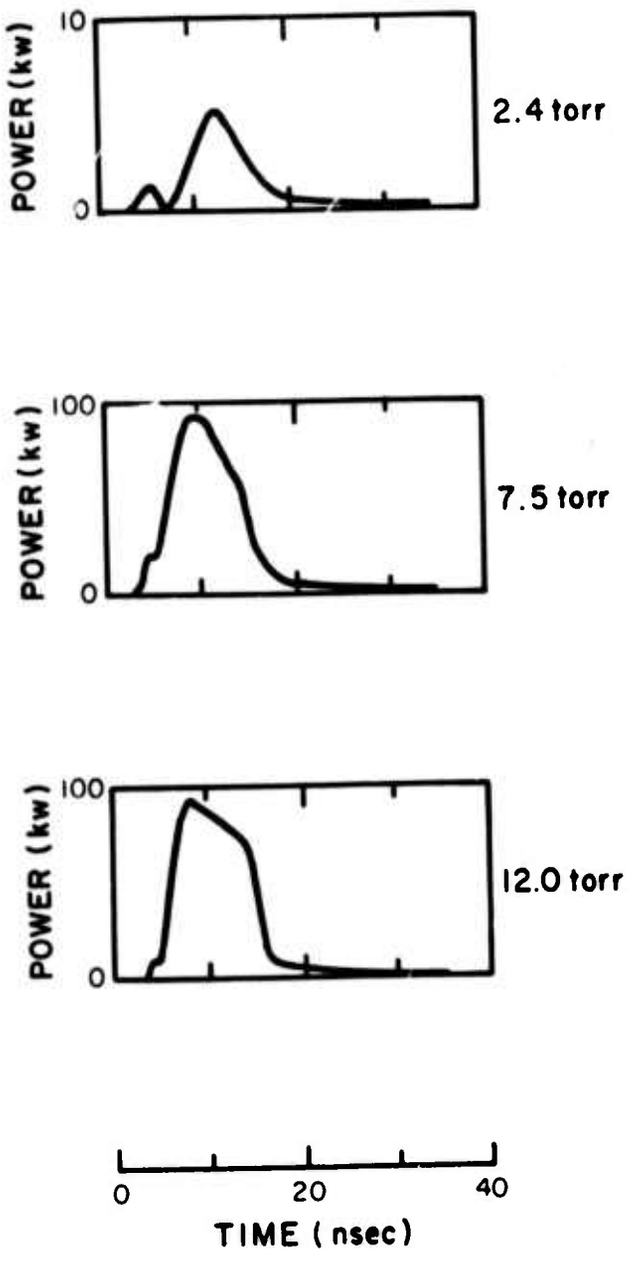
10
POWER (kw)
0
2.4 torr
100
POWER (kw)
0
7.5 torr
100
POWER (kw)
0
12.0 torr
0
20
40
TIME (nsec)

lowest partial pressure shown, 2.4 Torr, the 3914 Å emission, corresponding to the first peak, is seen to quench the total power output for several nanoseconds following its self-termination.

The problems of determining the absolute energy deposition from the electron beam in the radiating volume are quite acute and resulting values are generally unconvincing at the present state-of-the-art. This makes the measurements of absolute efficiency of the laser output difficult and generally dependent on various assumptions about electron trajectories in the high pressure gases. An attractive approach to the problem is made by the comparison of relative efficiencies of the different e-beam lasers excited under sufficiently similar conditions to allow cancellation of the most arbitrary factors. It appears that such comparisons of the relative efficiency of different nitrogen laser types offers a particularly useful normalization of the measurements just presented.

It is clear from the material presented in Section II that a particularly significant parameter to normalize around is the total energy deposition at the time of energy extraction. Considering equations (8) and (11) the total energy deposition at the time of energy extraction, T, can be approximately expressed as a geometric factor ω times the product of pressure and stopping power integrated from o to T, as

$$\varepsilon(T) = \omega P \int_o^T \frac{dE}{dx} \, dt \quad . \tag{38}$$

More simply

$$\varepsilon(T) = \omega P \left(\frac{dE}{dx}\right) T, \tag{39}$$

where now the variation of dE/dx has been absorbed in the constant, ω.

lowest partial pressure shown, 2.4 Torr, the 3914 Å emission, corresponding to the first peak, is seen to quench the total power output for several nanoseconds following its self-termination.

The problems of determining the absolute energy deposition from the electron beam in the radiating volume are quite acute and resulting values are generally unconvincing at the present state-of-the-art. This makes the measurements of absolute efficiency of the laser output difficult and generally dependent on various assumptions about electron trajectories in the high pressure gases. An attractive approach to the problem is made by the comparison of relative efficiencies of the different e-beam lasers excited under sufficiently similar conditions to allow cancellation of the most arbitrary factors. It appears that such comparisons of the relative efficiency of different nitrogen laser types offers a particularly useful normalization of the measurements just presented.

It is clear from the material presented in Section II that a particularly significant parameter to normalize around is the total energy deposition at the time of energy extraction. Considering equations (8) and (11) the tot energy deposition at the time of energy extraction, T, can be approximately expressed as a geometric factor ω times the product of pressure and stopping power integrated from o to T, as

$$\varepsilon(T) = \omega P \int_o^T \frac{dE}{dx} \, dt \quad . \tag{38}$$

More simply

$$\varepsilon(T) = \omega P \, \frac{dE}{dx} \, T, \tag{39}$$

where now the variation of dE/dx has been absorbed in the constant, ω.

The deposition time, T, must be determined and since it is the intent to compare the nitrogen ion laser operating in helium with the nitrogen-argon excitation transfer laser, the time dependence of both laser outputs must be compared. Figure 21 shows a comparison made from excitation of 7 atm. of helium containing 8 Torr nitrogen and 7 atm of argon containing 646 Torr nitrogen, both excited by e-beam pulses reaching peak currents of 14 KA. In each case shown the optical cavity and detector geometries are the same, and only the mirror coatings differ. Partial pressures of nitrogen were individually optimized for the total pressure of 7 atm common to both systems. It appears the deposition times can be estimated from the times required for the outputs to fall to 1/e of their peak values and these points are shown in the figure as they typically occur.

As shown in Figure 22, although the peak power output is a strong function of total pressure, the deposition time is not and the values shown in Figure 21 were chosen as suitably representative of all total pressures examined.

Finally choosing a normalization point so that both T and dE/dx at one atmosphere equal unity for helium, the relative deposition for helium is made numerically equal to the total gas pressure in atmospheres. The relative dE/dx for argon is unambiguously equal to 7.5 over the range of beam energies of importance[9] and this together with the relative T from Figure 21 make the relative deposition of energy in argon numerically equal, on the same scale, to 10.3 times the pressure in atmospheres.

Figure 23 summarizes the results of measurements of total laser pulse energy output as a function of the relative deposition of energy from the electron beam. On such a log-log plot, lines of constant efficiency appear as diagonals and are free from most arbitrary assumptions regarding the magnitude of the absolute energy deposition.

Figure 21

Time resolved total power measurements of the laser output pulses from optical cavities individually optimized for the gas mixtures indicated to the right of each trace. In each case total gas pressure was 7 atm. Partial pressures of nitrogen were 8 and 646 Torr for the helium and argon systems, respectively. The time scale is indicated below and has been zeroed to the initiation of the e-beam current. The time at which laser output falls to 1/e of its peak value is indicated. Peak e-beam current was 14 KA.

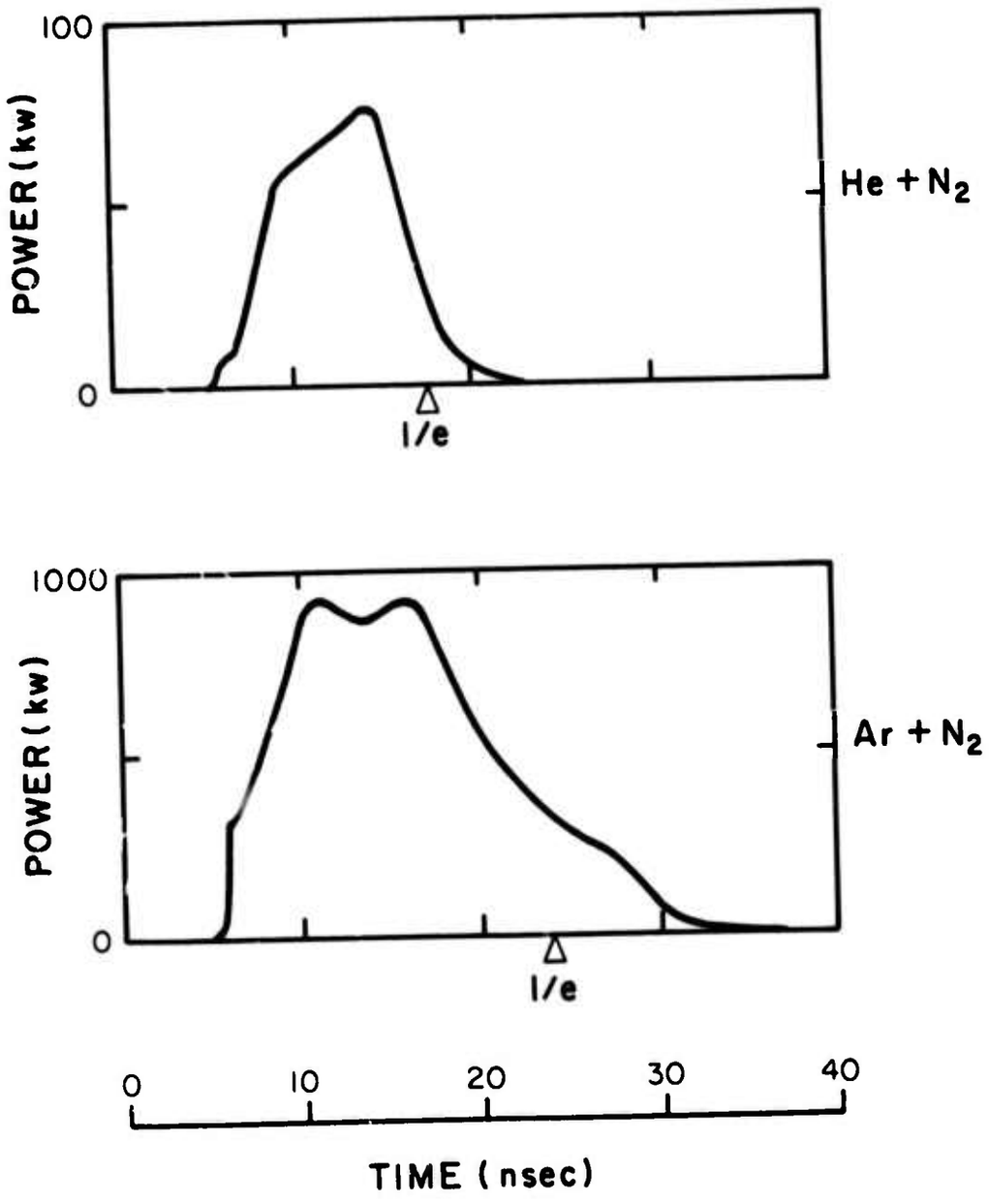
100
POWER (kw)
0
1/e
He + N2
1000
POWER (kw)
0
1/e
Ar + N2
0
10
20
30
40
TIME (nsec)

Figure 22

Time resolved measurements of power emitted from the nitrogen ion laser at various total pressures. In each case the partial pressure of nitrogen was 8 Torr and the total pressure of helium and nitrogen is shown to the right of each trace. The time scale is shown and has been zeroed to coincide with the initiation fo the e-beam current pulse. Peak e-beam current was 14 KA.

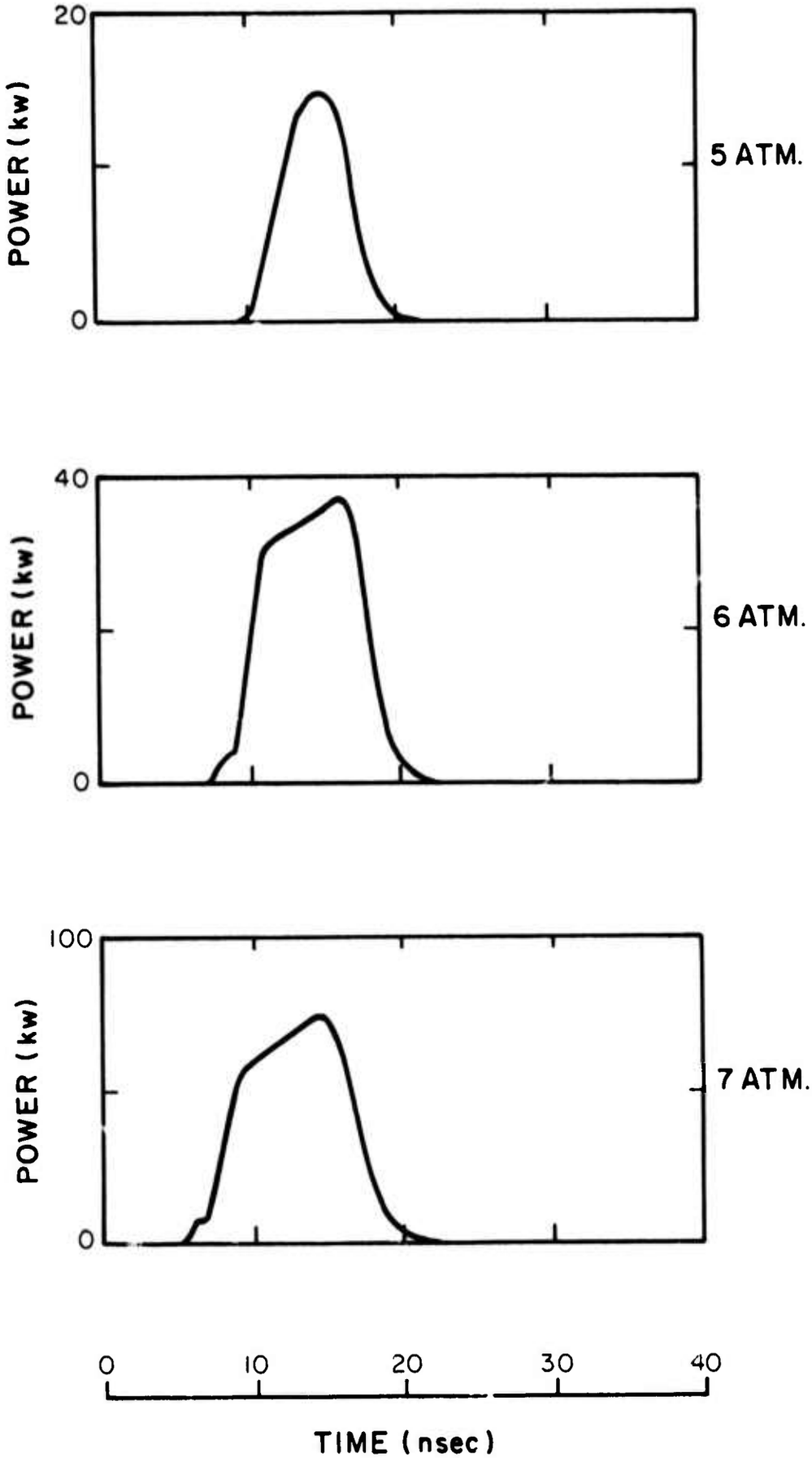
20
POWER (kw)
0
5 ATM.
40
POWER (kw)
0
6 ATM.
100
POWER (kw)
0
7 ATM.
0
10
20
30
40
TIME (nsec)

Figure 23

Summary plot of total laser pulse energy emitted from a 25 cm^3 volume as a function of relative deposition of energy from the electron beam. Variation of the deposition is obtained by changing the total gas pressure and, hence the stopping power. The peak e-beam current is 14 KA in each case. Lines of constant efficiency appear as diagonals.

○ - Helium containing 8 Torr nitrogen

□ - Helium containing 20 Torr nitrogen

△ - Argon containing 646 Torr nitrogen

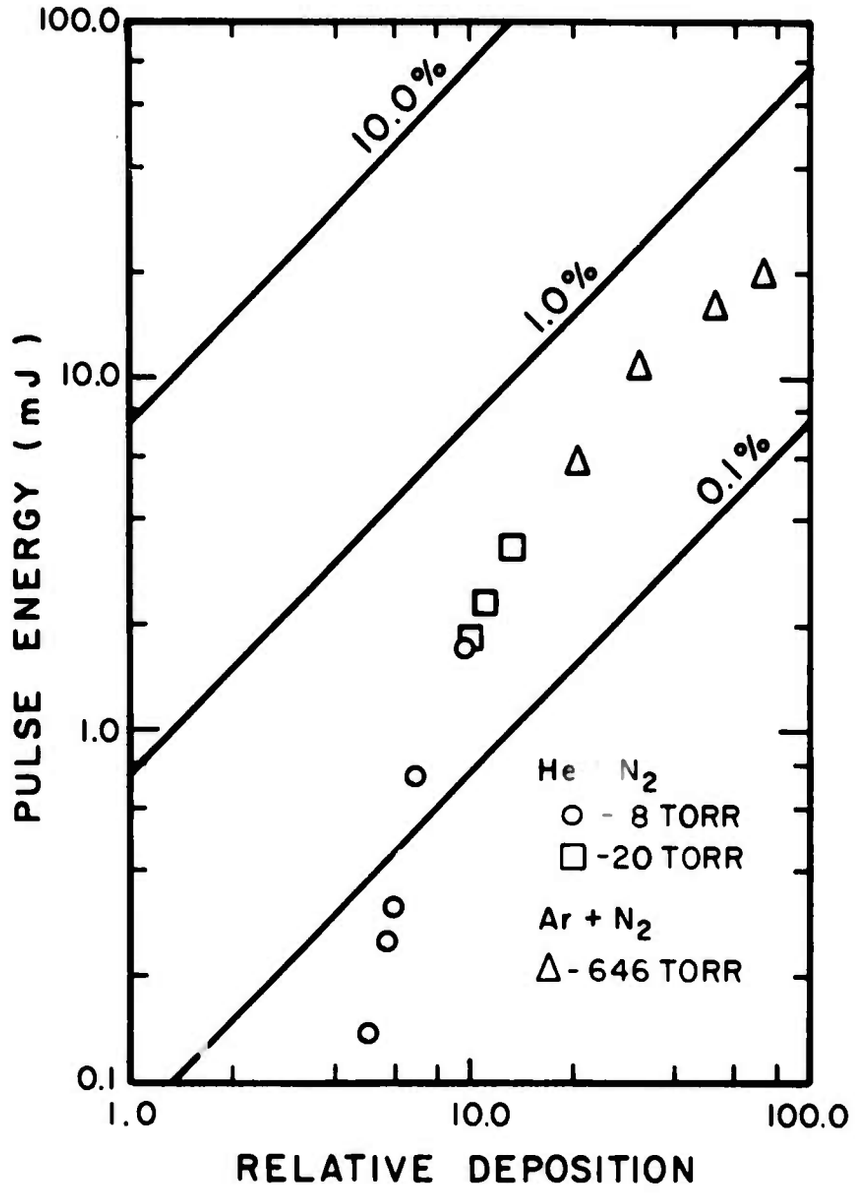
100.0
10.0
1.0
0.1
PULSE ENERGY (mJ)
10.0%
1.0%
0.1%
He + N2
○ - 8 TORR
□ -20 TORR
Ar + N2
Δ - 646 TORR
1.0
10.0
100.0
RELATIVE DEPOSITION

As can be seen in the case of the nitrogen ion laser in helium, not only the pulse energy, but also the efficiency increases strongly with energy deposition, most probably as a consequence of the unblocking of the lower state by collisional processes involving the free electrons. Since the lower laser state is a molecular ion, N_2^+, this process might be dissociative recombination.

If an absolute calibration is desired, the analytical methods of Section II and in particular equation (20) yield a calibration constant of 76 milli-Joules per relative deposition unit in the 25 cm^3 working volume. This constant has been used to construct the lines of constant efficiency shown in Figure 23. It can be seen that 13.5 atm pressure of helium the nitrogen ion laser has reached an efficiency of around 0.3% at a peak power of 325 KW for a 10 nanosecond pulse at 4278 Å. This is essentially the same efficiency seen for the argon-nitrogen laser operated at relative depositions ranging from 20 to 70.

VI. IMPLICATIONS

The high efficiency already observed in the emission of the single line at 4278 Å from the first nitrogen ion laser confirms the importance of the charge transfer pumping mechanisms proposed by the Principal Investigator and co-workers.[1] Moreover, it points toward the development, in the visible wavelength region, of new types of high energy lasers depending upon charge transfer from electron beam excitation of analogous high pressure gas mixtures. It should be emphasized that it is reasonable to expect that this will ultimately lead to the construction of lasers operating with efficiencies between 5 and 10% at a variety of wavelengths in the visible region.

More immediate implications concern the further scaling of the current test laser device. If satisfactory scaling with beam current can be demonstrated in future tests of larger volumes, it is reasonable to expect that a factor of 30 can be immediately achieved in energy density output from the existing device. A factor of 7 can be expected to result from increasing the beam current from 13.4 to the maximum 100 KA and another 2 from increasing the pressure to 30 atm. In this case, even with no further optimization of efficiency, an output energy of 1.8 Joules/liter at 4278 Å can be expected.

If the efficiency continues the increasing trend shown in Figure 23, it is not unreasonable to expect it to reach 1% by a relative deposition of 210. In this case 6 Joules/liter at 4278 Å would be expected. For a 10 nanosecond output pulse, this would suggest a peak power of 600 Megawatts could be obtained from a laser with a one-liter active volume.

It is further reasonable to expect that this energy can be switched into other radiative channels from the same upper state through the use of

mirror sets of appropriate reflectivity at the desired wavelength and suitably transparent at the others. Since the three potentially useful wavelengths lie at 427, 471 and 523 nm, they are sufficiently separated that fabrication of such mirror sets should present no technological problem.

Finally, it appears that, if development along those lines appeared warranted, a visible laser of exceptionally high average power could be pumped by charge transfer. Assuming, again, that the test laser system proves scalable, it can be expected that some type of sustainer excitation could be arranged to pump of the order of 5 liters at the 1.4 KA/cm^2 current density with a repetition rate of 100 pps. Then, at 30 atmospheres pressure, a laser with 130 watts average power at 4278 Å could be realized at the 0.3% efficiency currently demonstrated or 430 watts if the 1% value of efficiency can be attained.

While such projections are, of course, speculative, these are the implications of the recent successes with the preliminary scaling of the first nitrogen ion laser discussed in this report.

VII. REFERENCES

1. C. B. Collins, A. J. Cunningham, S.M. Curry, B.W. Johnson and M. Stockton, Appl. Phys. Lett. 24, 477 (1974).

2. C.B. Collins, A.J. Cunningham and M. Stockton, Appl. Phys. Lett. 25, 344 (1974).

3. J.B. Gerardo and A.W. Johnson, I.E.E.E., J. Quant. Elec. QE-9, 748(1973).

4. M.L. Bhaumik and E.R. Ault, U.V. Gas Laser Studies Special Technical Report (Northrop Corp. NRTC. 73-16R, (1973).

5. R.W. Dreyfus and R.T. Hodgson, Appl. Phys. Lett. 20, 195 (1972).

6. R.T. Hodgson and R.W. Dreyfus, Phys. Rev. Lett. 28, 536 (1973).

7. D.A. Hammer and N. Rostoker, Phys. Fluids 13, 1831 (1970).

8. R.V. Lovelace and R.M. Sudan, Phys. Rev. Lett. 27, 1256 (1971).

9. G. Knop and W. Paul, in: Alpha, Beta and Gamma-Ray Spectroscopy (ed. Kai Siegbahn, North-Holland Co., Amsterdam, 1965), p 1-25.

10. C.B. Collins and A. J. Cunningham, The Nitrogen Ion Laser, Special Technical Report, UTDP-ML-01 (1974).

11. W.P. Jesse and J. Sadauskis, Phys. Rev. 97, 1668 (1955).

12. C.B. Collins and W. W. Robertson, J. Chem. Phys. 40, 701 (1964).

13. R.A. Gerber, G. F. Sauter and H.J. Oskam, Phys. Lett., 19, 656 (1966).

14. D. K. Bohme, N.G. Adams, M. Mosesman, D.P. Dunkin, and E.E. Ferguson, J. Chem. Phys. 52, 5094 (1970).

15. F.C. Fehsenfeld, P.D. Goldan, A. L. Schmeltekopf, H.I. Schiff, and E.E. Ferguson, J. Chem. Phys. 44, 4087 (1966).

16. G. Herzberg, Molecular Spectra and Molecular Structure: I. Spectra of Diatomic Molecules (Van Nostrand, Princeton, N.J., 1950), p. 21.

17. D.C. Tyte and R.W. Nichols, Identification Atlas of Molecular Spectra, University of W. Ontario, Dept. of Physics, Molecular Excitation Group, London, Ont. 1965 p. 14.

18. G. Herzberg, op. cit., p. 125.

19. G. Herzberg, op. cit., p. 554.

20. R. W. Nicholls, J.Res. NBS, 65A, 451, (1961).

21. M. L. Bhaumik, E.R. Ault, and N.T. Olson, U.V. Gas Laser Investigations Semiannual Technical Report (Northrop Corp. NRTC. 74-26R, (May 1974)).

References (cont'd)

22. C.B. Collins, A.J. Cunningham, S.M. Curry, B.W. Johnson and M. Stockton, Appl. Phys. Lett. 24, 245 (1974).

23. C.B. Collins and A.J. Cunningham, Recombination Laser, Report No. UTDP A002-4, ONR Contract No. N00014-67-A-0310-0007, 1974.